A parametric study of cochlear input impedance

Sunil Puria, and Jont B. Allen

Citation: The Journal of the Acoustical Society of America **89**, 287 (1991); doi: 10.1121/1.400675
View online: https://doi.org/10.1121/1.400675
View Table of Contents: http://asa.scitation.org/toc/jas/89/1
Published by the Acoustical Society of America

A parametric study of cochlear input impedance[a)]

Sunil Puria
AT&T Bell Laboratories, Murray Hill, New Jersey 07974 and The City College of CUNY, Department of Electrical Engineering, New York, New York 10031

Jont B. Allen
AT&T Bell Laboratories, Murray Hill, New Jersey 07974

(Received 3 November 1989; revised 4 September 1990; accepted 19 September 1990)

In this paper various aspects of the cat cochlear input impedance $Z_c(\omega)$ are implemented using a transmission line model having perilymph viscosity and a varying cross-sectional scalae area. These model results are then compared to the experimental results of Lynch *et al.* [J. Acoust. Soc. Am. **72**, 108–130 (1982)]. From the model, the following observations are made about the cochlear input impedance: (a) Scalae area variations significantly alter the model $Z_c(\omega)$; (b) the use of anatomically measured areas improves the fits to the experimental data; (c) improved agreement between model and experimental phase is obtained when perilymph viscosity and tapering are included in the cochlear model for frequencies below ≈ 150 Hz; (d) when model scalae tapering and perilymph viscosity are chosen to match physiological conditions, the effect of the helicotrema impedance on $Z_c(\omega)$ is insignificant; and (e) the cochlear map, which is defined as the position of the basilar membrane peak displacement as a function of stimulus frequency, can have an important effect on $Z_c(\omega)$ for frequencies below 500 Hz. A nonphysiological cochlear map can give rise to cochlear standing waves, which result in oscillations in $Z_c(\omega)$. Scalae tapering and perilymph viscosity contribute significantly to the damping of these standing waves. These observations should dispel the previous notion that $Z_c(\omega)$ is determined solely by parameters of the cochlea close to the stapes, and the notion that $Z_c(\omega)$ is dominated by the helicotrema at low frequencies.

PACS numbers: 43.64.Kc, 43.64.Bt

LIST OF SYMBOLS

A,B,C,D	elements of the 2×2 two-port chain matrix
A_{fp}	area of footplate (cm^2)
$\beta(x)$	basilar membrane (BM) width $[\beta_0 \exp(\beta_1 x)]$ (cm)
β_0	BM width at the base (cm)
β_1	rate of change parameter of the BM width (cm^{-1})
c	velocity of sound in water (cm/s)
$C(x)$	capacitive component of Y
δ	viscous boundary layer thickness
Δ	space discretization length (cm)
f	frequency (Hz)
$f_{CF}(x)$	cochlear map
F_v,F_t	complex functions
γ	ratio of specific heats
$G(x)$	conductive component of Y
$\Gamma(x)$	propagation constant (cm^{-1})
j	$\sqrt{-1}$
J_n	complex Bessel functions of order n
$K_b(x),K_b'(x)$	BM specific stiffness (dyn/cm^3)
K_{rw}	round window stiffness (dyn/cm^5)
$L(x)$	inductive component $[L_0 + L_v]$ of Z
$L_0(x)$	component of L due to fluid inertia
$L_v(x)$	component of L due to fluid viscosity
$M\Omega$	10^6 dyn − s/cm^5
n_p	number of sections of x_L
η	coefficient of viscosity (g cm^{-1} s^{-1})
ρ	mass density of perilymph (g/cm^3)
$P(x)$	pressure difference across BM partition (dyn/cm^2)
$R_v(x)$	resistive component of Z
$r_0(x)$	tube radius
r_v	ratio of the tube radius to viscous boundary layer thickness
r_t	ratio of the tube radius to thermal boundary layer thickness
s	$j\omega$
$S(x)$	scala area (cm^2)
$S_V(x)$	scala vestibule area
$S_T(x)$	scala tympani area
S_0	scala area at the base (cm^2)
s_1	rate of change parameter for scala area (cm^{-1})
$U(x)$	volume velocity through scala (cm^3/s)
u_{st}	particle velocity of stapes (cm/s)
$V_{BM}(x)$	BM volume velocity (cm^3/s)
ω	angular frequency ($2\pi f$)
x	distance from stapes (cm)
x_L	length of cochlea (cm)
$Y(x)$	per unit length shunt acoustic admittance (cm^4 dyn^{-1} s^{-1})

[a)] Portions of this paper were presented at the 116th Meeting of the Acoustical Society of America in Honolulu, HI [J. Acoust. Soc. Am. Suppl. 1 **84**, S54 (1988)] and also at the Association for Research in Oto-Laryngology Meeting [Assoc. Res. Oto-Laryngol. Abstr. **12**, 142 (1989)].

 0001-4966/91/010287-23$00.80

$Y'(x)$	BM acoustic admittance per unit length ($cm^4\ dyn^{-1}\ s^{-1}$)
$Z(x)$	per unit length series acoustic impedance $[R_v + sL]$ (dyn − s/cm^6)
$Z'(x)$	equivalent impedance per unit length for the two chambers [Eq. (1)]
$Z_{BM}(x)$	BM trans-membrane specific impedance [Eq. (1)] [(dyn − s/cm^3)
$Z_c(\omega)$	complex cochlear input impedance [Eq. (10)] (dyn − s/cm^5)
$Z_{crw}(\omega)$	Z_c with the round window impedance added in series [Eq. (19)]
$\lvert Z_c\rvert, \lvert Z_{crw}\rvert$	magnitude of Z_c and Z_{crw}
$\angle Z_c, \angle Z_{crw}$	phase of Z_c and Z_{crw}
$Z_a(x), Z_b(x)$	elements of the T network [Eq. (7a)] (dyn − s/cm^5)
Z_h	acoustic impedance of helicotrema [Eq. (11)] (dyn − s/cm^5)
$Z_0(x)$	characteristic impedance of tube (dyn − s/cm^5)

INTRODUCTION

Many aspects of cochlear models are known to fail at low frequencies (i.e., below 500 Hz). These problems become worse as the frequency decreases. As the traveling wave approaches the end of the cochlea, the apical boundary condition becomes important. An improper boundary condition leads to apical reflections of the traveling wave. These model failures are most easily seen by studying the cochlear input impedance where many of the model pathologies manifest themselves. While cochlear input impedance for animals shows no indication of apical reflections at low frequencies, model cochlear input impedance data show the presence of high-Q (f_0/bandwidth) cochlear resonances or cochlear standing waves for frequencies below 500 Hz (Matthews, 1980). A presence of these standing waves in nonlinear cochlear models would likely result in other serious artifacts that could confound further interesting results. To our knowledge, there does not exist any study in the cochlear modeling literature on how to eliminate these resonances. Most previous one-dimensional cochlear models (Peterson and Bogert, 1950; Zwislocki, 1950), two-dimensional cochlear models (Lesser and Berkley, 1972; Sondhi, 1978), nonlinear cochlear models (Hall, 1974), active models (Neely and Kim, 1986), and nonlinear active models (Diependaal, 1988) have assumed a cochlea map of the form $f_{CF}(x) = A\,[10^{-\alpha/x_L(x-x_L)}]$. Standing waves exist under the condition of large reflection coefficients at the stapes end and at the apical end of the cochlea. In this paper, we shall show how standing waves, as seen in Z_c, are related to the cochlear map, scalae tapering, viscosity, and the helicotrema impedance.

A second problem concerns the magnitude and phase of the cochlear input impedance at low frequencies. Previous cochlear models indicate that the cochlear input impedance significantly decreases in magnitude for frequencies below about 1 to 2 kHz. For the cat, models and experimental magnitude data of Lynch *et al.* (1982) are in disagreement by as much as 16 dB at 50 Hz. In the real cochlea, the scalae are tapered, with a decreased area at the apex. Also, in the real cochlea, the scalae fluids are viscous. These scalae-area changes and viscous losses play an important role at low frequencies (Koshigoe *et al.*, 1983). Only by including scalae tapering and viscosity can we hope to overcome the nonrealistic standing waves and hope to accurately model the cochlear input impedance at low frequencies.

In summary, there is a poor general understanding of low-frequency phenomena in the cochlea. In this paper we investigate low-frequency cochlear phenomena by modeling the cochlear input impedance.

There are other reasons besides low-frequency modeling questions that motivate us to study the cochlear input impedance. *First,* the mechanical "load" on the middle ear is the input impedance of the cochlea $Z_c(\omega)$. Inaccurate representations of Z_c will result in the middle-ear model parameters that are not representative of the physical system. A good model for Z_c is necessary to estimate the middle ear parameters accurately (Moller, 1965).

Second, accurate knowledge of Z_c is crucial for the energy flow consideration in the forward and reverse directions. The acoustic energy in the ear canal normally propagates toward the cochlea. There have been many observations made in the ear canal indicative of nonlinear, and perhaps active, acoustic emissions originating in the cochlea. These emissions result from a reverse energy flow from the cochlea to the ear canal. Examples include the cubic difference tones resulting from nonlinearities within the cochlea (Wilson, 1980; Kim *et al.*, 1980; Fahey and Allen, 1985), as well as spontaneous and evoked otoacoustic emissions observed by Kemp (1978, 1979), Zurek (1981), and others. The impedance mismatch at the cochlea–stapes boundary reflects back some of the acoustic emissions generated in the organ of Corti (Kemp, 1980). The rest of the energy passes through the middle ear and appears in the ear canal. To estimate the reflection and transmission of energy at the cochlea–stapes interface, it is necessary to have a good model of the middle ear and of the cochlear input impedance.

The paper is organized as follows. In Sec. I we review previous models and measurements of cochlear input impedance. In Sec. II we formulate the model equations. Section III A shows the effects of various cochlear maps on Z_c. In Sec. III B, the effects of viscosity and the helicotrema on Z_c are analyzed, assuming a constant scalae area. Section III D shows the effects of scalae tapering on Z_c, and the interactions of tapering with viscosity and the helicotrema. Section III F compares measured data and the model with tapering and viscosity. Resulting comparisons to the Lynch *et al.* experimental data are also shown in Sec. III F for several

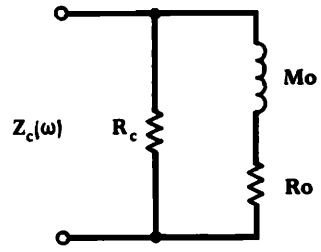

FIG. 1. Many previous models of Z_c can be generalized by this lumped parameter circuit. The values for R_c, R_0, M_0 and the mechanisms corresponding to them are listed in Table I.

choices of parameter variations. In Sec. IV, $Z_c(\omega)$ for the cat, man, guinea pig, and the chinchilla are compared. A discussion of the results can be found in Sec. V, followed by a summary in Sec. VI.

I. PREVIOUS WORK

Figure 1 shows the Lynch *et al.* (1982) lumped network representation of the cochlear input impedance, which encompasses many previous models. It is an electrical analog of the mechanical system under consideration with voltage corresponding to pressure and current to volume velocity. In Table I we summarize the results of numerous research vis-à-vis the model of Fig. 1. Lynch *et al.* (1982) estimated parameters for the network of Fig. 1 based on averaged experimental input impedance data. We start from the Lynch *et al.* model because the experimental data on which that model is based is the most comprehensive.This makes their network model a good reference point for comparisons. In Fig. 1, R_c represents the cochlear impedance at high frequencies. At low frequencies, Z_c is given by the parallel combination of R_c and R_0. A transition region exists, which is between 10 and 200 Hz, where the mass M_0 has an effect.

Based on modeling considerations, Zwislocki (1965)

TABLE I. Comparison of Z_c by various researchers. Figure 1 is a companion figure to this table. The model of Z_c by Zwislocki, based on mathematical considerations, is a pure resistor R_c. Dallos' model, builds on Zwislocki's model by adding the series combination of mass of the helicotrema M_0 and damping of the helicotrema R_0 in parallel with R_c. Allen derived a model for Z_c based on the WKB approximation to the one-dimensional formulation of the cochlea. Allen's model is also the one of Fig. 1, but with $R_0 = 0$. Since $R_0 = 0$ in Allen's model, $\lim_{f\to 0} |Z_c| \to 0$ and $\lim_{f\to 0} \angle Z_c \to \pi/2$. Figure 1 is also the Lynch *et al.* model, based on measured data. In that model, $\lim_{f\to 0} |Z_c| \to R_c \| R_0$, and $\lim_{f\to 0} \angle Z_c \to 0$, due to the presence of R_0. Thus there is a low-frequency discrepancy in the theoretical models of Z_c and the measured data. This discrepancy is most significant for frequencies below 1 kHz, and is as large as 20 dB at 10 Hz. Based on approximate solutions to a one-dimensional formulation of the cochlea, Koshigoe *et al.* conjectured that this low-frequency discrepancy in Z_c is due to the effects of viscosity. In addition to not providing a good fit to the measured data, the Koshigoe *et al.* model does not attribute any physical mechanism(s) to R_0. However, they first argued that it is important to incorporate tapered scalae area in model calculations.

Reference	Model	Parameter R:dyn − s/cm^5 M: g/cm^4	Physical or physiological basis
Zwislocki (1965)	Fig. 1	$R_c = \sqrt{2\rho K_0/\beta_0 S_0}$ $R_0 = M_0 = \infty$	BM compliance and scala area at base
Tonndorf *et al.* (1966)			measured $\lvert Z_c\rvert$ data for the cat
Dallos (1970)	Fig. 1	R_c: as per Zwislocki R_0, M_0 species dependent [see Eq. (11)]	R_0, M_0 due to helicotrema
Sondhi (1978)	numerical calculation	similar to WKB (see Fig. 6)	from one- and two-dimensional cochlear models
Allen (1979)	Fig. 1	$R_c = 2\rho c_0/S_0 = \sqrt{2\rho H K_0/S_0^2}$ $R_0 = 0$, $M_0 = 8\rho/S_0 k_1$	derived from WKB
Dancer and Franke (1980)			measured $\lvert Z_c\rvert$ data for the guinea pig
Lynch *et al.* (1982)	Fig. 1	$R_c = 1.2\times 10^6$ $R_0 = 0.28\times 10^6$, $M_0 = 2250$	phenomenological: based on measured data for the cat
Koshigoe *et al.* (1983)	$R + sM$	$R = R_0(\omega)$, $M = M_0(\omega)$	Z_{BM}, viscosity, and constant cross-sectional area
Koshigoe *et al.* (1983)	numerical calculation	see Fig. 11	Z_{BM}, viscosity, and tapered cochlea

estimated $Z_c(\omega)$ to be real and of value $R_c = \sqrt{2\rho K_0/\beta_0 S_0}$, as shown in Table I.

Tonndorf *et al.* (1966) measured $|Z_c|$ for the cat and showed it to be frequency dependent. They found a 6-dB/oct slope for frequencies below 400 Hz. Near 400 Hz, $|Z_c|$ was approximately 8 $M\Omega$ (10^6 dyn $-$ s/cm^5). Above 400 Hz, $|Z_c|$ decreased, and, at approximately 1 kHz, tended to fluctuate between 2–5 $M\Omega$. The maximum error they reported was a factor of 3 ($\pm$ 9.5 dB). Dancer and Franke (1980), on the other hand, did not find a low-frequency slope in their measurements of the guinea pig cochlear input impedance magnitude.

Dallos' (1970) model closely resembles the Lynch *et al.* (1982) model. The physical basis for R_0 and M_0, as hypothesized by Dallos, is the viscosity and mass of the helicotrema, with the transition region being between 100 Hz and 1 kHz. In cochlear modeling, the helicotrema boundary condition has always been a point of conjecture. We shall show that, when we assume physiologically reasonable parameters, this boundary condition has a negligible effect.

Allen's (1979) derivation of Z_c is based on the Wentzel–Kramers–Brillouin (WKB) solution. The WKB solution was formulated for constant scalae area, zero perilymph viscosity, no reflections, and no helicotrema. Allen's Z_c is different from the Lynch *et al.* model to the extent that $R_0 = 0$. It is the inclusion of R_0 in the Lynch *et al.* model that gives rise to the behavior of Z_c below 200 Hz. From Table I we see that the WKB R_c is given by $2\rho c_0/S_0$, where c_0 is the speed of the traveling wave on the basilar membrane at the stapes and the area at the base is $S_0 = S(0)$. By substituting the value for c_0, it is easy to show that the WKB R_c is equivalent to Zwislocki's radiation resistance R_c. At low frequencies, the WKB input impedance is dominated by the mass given by $M_0 = 8\rho/(S_0 k_1)$, which depends on the rate of change parameter k_1 of the BM stiffness at the stapes. In this model, the cochlear input impedance depends only on the physical parameters of the cochlea in the neighborhood of the stapes.

Sondhi's (1978) numerical calculations of Z_c from one- and two-dimensional cochlear models are qualitatively similar to the WKB solutions for Z_c.

It is natural to consider what physical mechanisms give rise to R_0 in Fig. 1. Can R_0 be accounted for by including scalae tapering and viscosity? Given that R_0 affects the very-low-frequency regions, it is reasonable that perhaps the source of its effect is in scalae viscous losses.

Koshigoe *et al.* (1983) provide a mathematical framework that addresses this issue. Their derivation of Z_c, in a cochlear model with viscosity and constant scalae area, consists of frequency-dependent parameters R_0 and M_0. However, since their results do not provide a reasonable fit to the measured input impedance data, and their expressions fail to give insight into the mechanisms that dominate at frequencies below 500 Hz, further analysis is in order. Koshigoe *et al.* also calculated Z_c for a tapered scalae area model, with and without viscosity. At frequencies below 500 Hz, their inviscid calculations indicate $|Z_c|$ to be four to five times *smaller* than those that include viscosity. We will show that this result is inconsistent with our own numerical calculations. However, they were the first to argue the importance of the tapered scalae in model calculations.

Throughout the paper we have made extensive use of the impedance model and data of Lynch *et al.* (1982). To qualitatively isolate the parameters that have the greatest influence on the cochlear input impedance, we initially use the averaged measured data and model results of Lynch *et al.* We then use their individual data in an attempt to understand the individual differences.

II. THE CHAIN-MATRIX FORMULATION FOR COCHLEAR MECHANICS

The cochlea, in most animals, is a spiral-shaped structure. It consists of three fluid-filled chambers called the scala vestibule, scala media, and the scala tympani. In this study we assume that the effect of the spiral shape on the acoustical properties of the cochlea are insignificant (von Békésy, 1960, p. 407; Viergever, 1978). Figure 2(a) shows a simpli-

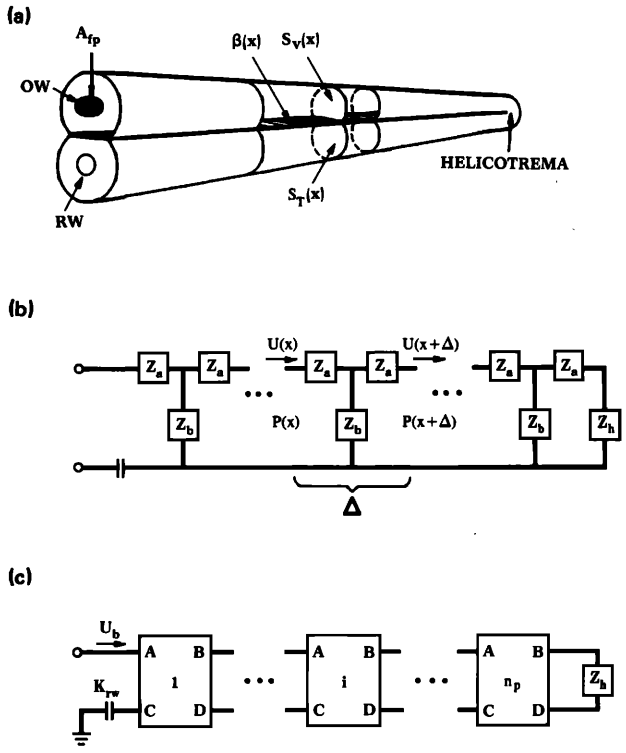

FIG. 2. (a) Approximate physical representation of the cochlea: $S_V(x)$ and $S_T(x)$ are the scala vestibule and scala tympani area functions, $\beta(x)$ is the basilar membrane (BM) width, RW is the round window, and OW is the oval window. The footplate, with area A_{fp}, is at the basal end of the cochlea and the helicotrema is at the apical end of the cochlea. Not shown here is the stapes that would have been attached to the footplate at the oval window. (b) Equivalent model in terms of "T" sections: The elements Z_a and Z_b are functions of position along the length of the cochlea. The cochlea is divided into n_p sections of length Δ cm. (c) Chain-matrix formulation of the physical model of (a): The matrices are formulated to include changes in scalae area, effects due to perilymph viscosity, and variations in the organ of Corti. U_b is the volume velocity at the base, K_{rw} is the round window stiffness, and Z_h is the impedance of the helicotrema.

fied sketch of the cochlea when it is uncoiled from its spiral shape. In Fig. 2(a), it is further assumed that the scala media is treated as part of the scalae vestibule. The two resulting chambers are separated by the organ of Corti, which is assumed to have a width $\beta(x)$. The scala vestibule area $S_V(x)$ and scala tympani area $S_T(x)$ are assumed to vary along the cochlear length. The distance x is measured from the stapes end. The basal end of the cochlea corresponds to $x = 0$ cm and the apical end of the cochlea corresponds to $x = x_L$ cm, where x_L is the total length of the cochlea. The scalae are divided into n_p cylindrical segments, each of length Δ cm. Under the assumptions of conservation of fluid mass and momentum, we obtain long-wave expressions for the pressure and volume velocity.

A. Some definitions

In the formulation of our model equations, several different types of impedances and admittances are required. There are two basic types of velocities in acoustics, namely, particle velocity and volume velocity. The volume velocity is given as surface integral over the particle velocity. Frequently, an equivalent uniform distribution of velocity is assumed, in which case the volume velocity is defined as the area times the effective particle velocity. The two different types of velocity lead to two different types of impedance, which are called *specific impedance*, and *acoustic impedance*. The specific impedance is given as the ratio of the pressure difference divided by the particle velocity, and has units dyn $-$ s/cm^3. The acoustic impedance is defined as the pressure difference divided by the volume velocity, which has units dyn $-$ s/cm^5. The cochlear input impedance Z_c, the helicotrema impedance Z_h, the characteristic impedance of a tube Z_0, and the series and shunt impedance of a "T" network Z_a and Z_b are all acoustic impedances. We must also define the series acoustic impedance Z and the shunt acoustic admittance Y for the lossy transmission line on a per unit length basis in units of dyn $-$ s/cm^6 and cm^4 dyn^{-1} s^{-1} (see Appendix A).

B. General approach

Starting from the basilar membrane impedance $Z_{BM}(x,\omega)$, the series impedance $Z(x,\omega)$, and shunt admittance $Y(x,\omega)$ from lossy transmission line theory, we would like to formulate the chain-matrix elements, $A(x_i,\omega)$, $B(x_i,\omega)$, $C(x_i,\omega)$, $D(x_i,\omega)$ [as shown in Fig. 2(c)]. The basilar membrane impedance $Z_{BM}(x_i,\omega)$ is given in terms of the physical variables relevant to the cochlea as described in Appendix B. From Z_{BM}, the BM width $\beta(x)$, and scalae area $S(x)$, we may find the shunt acoustic basilar membrane admittance per unit length $Y'_{BM}(x_i,\omega)$. The lossy transmission line impedance Z and shunt admittance Y are described in Appendix A. We then find Z' and Y', which are the cochlear two-chamber series acoustic impedance per unit length, and the shunt total lossy acoustic admittance per unit length. These allow us to find Γ and Z_0, the propagation constant and characteristic impedance, for the lossy cochlear transmission line. Next, we find the T elements Z_a and Z_b [see Fig. 2(b)], and finally the chain-matrix elements A, B, C, and D, which can be expressed in terms of the T elements.

C. Lossy BM series impedance

The equation for the series impedance $Z(x,\omega)$ [Eq. (A1)] is for a single vestibule. Anatomical measurements of scala vestibule cross-sectional area $S_V(x)$ and scala tympani cross-sectional area $S_T(x)$ on humans indicate the areas of the two vestibules to be approximately equal for distances greater than 0.3 cm from the round window (Wever, 1949, pp. 276–278). Thus we will assume $S(x) = S_v(x) = S_T(x)$. The series impedance for a two-chamber model then is

$$Z' = 2Z. \tag{1}$$

The two impedances Z and Z' are given as per unit length series acoustic impedances (dyn $-$ s/cm^6) along the vestibule.

D. Lossy BM shunt admittance

To find the lossy transmission line shunt admittance for the cochlea, we must modify Y of Appendix A to include the shunt admittance due to the basilar membrane. The basilar impedance $Z_{BM}(x,\omega)$ is a specific impedance (dyn $-$ s/cm^3). From a macromechanical point of view, Z_{BM} consists of BM stiffness $K_b(x)$, damping, and mass. $Z_{BM}(x)$ is a physically motivated, micromechanical model of BM specific impedance that incorporates a resonant tectorial membrane (Allen, 1980) and that leads to a fourth-order equation for partition dynamics. These parameters depend on the cochlear map as shown in Appendix B.

The shunt admittance due to viscous losses Y and the shunt admittance due to the basilar membrane Y'_{BM} are in per unit length acoustic admittances (cm^4 dyn^{-1} s^{-1}). The BM impedance $Z_{BM}(x,\omega)$, when transformed[1] to basilar membrane acoustic admittance per unit length is

$$Y'_{BM}(x,\omega) = S_0/HZ_{BM}(x,\omega). \tag{2}$$

Thus the total lossy transmission line acoustic admittance per unit length is found by adding the two admittances together:

$$Y' = 2Y + Y'_{BM}. \tag{3}$$

The factor of 2 accounts for the admittance due to the two chambers.

Equation (2) is the BM acoustic admittance per unit length. Model parameters and physical measurements of the BM are often given in terms of BM specific impedance. For our model we use

$$Z'_{BM} = \beta(x)/Y'_{BM}. \tag{4}$$

In this equation the transformed BM stiffness is $K'_b(x)$. The basilar membrane stiffness at the base is defined as $K'_0 = K'_b$ $(x = 0)$.

E. Effect of fluid compression

For most fluids, including perilymph, the ratio of specific heats $\gamma \simeq 1$, and thus $G(x,\omega)$ of Eq. (A5) is zero; consequently, $Y(x,\omega)$ in Eq. (3) reduces to $sC(x)$.

The compliance $C(x) = S(x)/\rho c^2$ is a measure of compressibility of the fluid. Near the base, $2C(x)$ is less than 6%

of the basilar membrane admittance, and, in the apical region, $2C(x)$ is at least three orders of magnitude smaller than Y'_{BM}. Although not shown here, the effect of including $s2C(x)$ in Eq. (3) on $|Z_c|$ was found to be less than 0.5 dB near 20 kHz. No differences were observed in $\angle Z_c$. For these reasons, we have used the approximation

$$Y' \approx Y'_{BM} \tag{5}$$

for all further calculations.

F. Transmission line parameters

Given Z' and Y', one may calculate the characteristic impedance Z_0 and the propagation constant Γ for the lossy cochlear transmission line:

$$Z_0(x,\omega) = (Z'/Y')^{1/2}, \tag{6a}$$

$$\Gamma(x,\omega) = (Z'Y')^{1/2}. \tag{6b}$$

Transformation to the equivalent cochlear T network of Fig. 2b is defined in terms of Z_a and Z_b as follows (Flanagan, 1983, Chap. 3):

$$Z_a(x,\omega) = Z_0 \tanh(\Gamma\Delta/2), \tag{7a}$$

$$Z_b(x,\omega) = Z_0 \operatorname{csch}(\Gamma\Delta). \tag{7b}$$

G. Chain-matrix form

The relationship for the pressure and volume velocity of each section of length Δ can now be put in *chain-matrix* form (Weinberg, 1962; Pierce, 1989):

$$\begin{bmatrix} P(x) \\ U(x) \end{bmatrix} = \begin{bmatrix} AB \\ CD \end{bmatrix} \begin{bmatrix} P(x+\Delta) \\ U(x+\Delta) \end{bmatrix}, \tag{8}$$

where elements of the *ABCD* chain matrix are

$$A = 1 + (Z_a/Z_b), \tag{9a}$$

$$B = Z_a[2 + (Z_a/Z_b)], \tag{9b}$$

$$C = 1/Z_b, \tag{9c}$$

$$D = A. \tag{9d}$$

Equation (8) relates the pressure difference and volume velocity of a cylindrical section at x given the pressure difference and volume velocity of a section at $x + \Delta$. Inherent in the formulation of Eq. (8) is a *forward and backward traveling wave.*.

Referring to Fig. 2(c), the chain is started at the helicotrema end by assuming $U(x_L) = 1$. The unit volume velocity results in a pressure drop $P(x_L)$ across $Z_h(\omega)$, the acoustic impedance of the helicotrema. Equation (8) is then recursively calculated with the space index decreasing from $x = x_L$ at the helicotrema end to $x = 0$ at the base, for n_p segments. $P(x)$ and $U(x)$ are finally normalized so that the calculated volume velocity at the base $U(0) = u_b S_0$, to satisfy the boundary condition in the base of the cochlea.

We use the chain-matrix method to do all the calculations for each of the n_p segments. The number of sections n_p was successively increased by a factor of 2 until no further change in the results were observed; this occurred at $n_p = 1024$. The computations were carried out on an Alliant FX/80 computer. To verify our chain-matrix method, we made comparisons of Z_c and the BM velocity calculated by solving Laplace's equation for the constant scalae height and zero viscosity case, using the difference equation[2] method (Allen, 1977). In making these comparisons, we discovered a helicotrema boundary condition problem at low frequency. This will be further discussed in Sec. II J. With this exception, calculations of the cochlear input impedance and BM volume-velocity were identical for the two methods.

H. Cochlear input impedance

The volume velocity that enters the stapes is $u_{st}A_{fp}$. By conservation of mass, this volume velocity is equal to the volume velocity entering the scala vestibule in the base $u_b S_0$. The cochlear acoustic input impedance is then calculated from

$$Z_c(\omega) = P(0)/u_{st}A_{fp}. \tag{10}$$

Measurements of pressure in the cat scala vestibule and scala tympani, as a function of the tympanic membrane sound-pressure level, and over a wide range of frequencies, have been found to be linear (Nedzelnitsky, 1980). With the tensor tympani muscle cut from the stapes, the mammalian middle ear acts as a linear system for sound-pressure levels of up to 130 dB SPL (Guinan and Peake, 1967). Therefore, we assume Eq. (10) to hold at all levels of input. The linearity assumption is not necessarily valid for all animals. For example, Rosowski *et al.* (1984) have found the acoustic input admittance at the alligator lizard tympanic membrane to be ear canal pressure dependent for stimulus levels greater than 70 dB SPL.

I. The helicotrema boundary condition

When formulating a cochlear model, one may assume different properties for the helicotrema. The two most common boundary conditions are the open circuit $Z_h = \infty$ and the short circuit $Z_h = 0$. A third choice is (Dallos, 1970) helicotrema model using a short-tube impedance (TI). In this paper we have limited ourselves to either the short-tube or short-circuit impedance boundary condition. The open-circuit assumption is nonphysiological since it does not allow for any flow between the two scalae.

The acoustic impedance of a tube of radius a_h and length l_h given by (Beranek, 1954, p. 135)

$$Z_h(\omega) = \frac{8\eta l_h}{\pi a_h^4} + j\left(\frac{4}{3}\right)\left(\frac{\rho l_h}{\pi a_h^2}\right)\omega. \tag{11}$$

This approximate formula is valid for $a_h(\text{cm}) < 0.2/\sqrt{f}$. Dallos (1970) used Eq. (11) for his calculations of Z_c. Mulroy (Lynch *et al.*, 1982, footnote 11) measured the helicotrema radius of the cat by scanning electron microscope techniques and found it to be 0.0125 ± 0.0005 cm. Using this radius, Eq. (11) is valid for $f < 256$ Hz. If we assume the helicotrema to be a bent circular tube of radius a_h as above, then the length of the helicotrema $l_h = \pi a_h \approx 0.04$ cm. The short-circuit condition will be referred to as $Z_h = \text{SC}$, and the tube impedance condition will be referred to as $Z_h = \text{TI}$ throughout the text.

J. The BM response

Although this is not explicitly a study of BM mechanics, an intermediate result is the BM volume velocity at any place along the length of the cochlea:

$$U_{\rm BM}(x,\omega) = [P(x+\Delta) + Z_a U(x+\Delta)]/Z_b, \quad (12)$$

where the terms of Eq. (12) are identified in Fig. 2(b). The BM center-line particle velocity, assuming a half-sine-shaped velocity distribution over the BM width, is

$$\overline{U}_{\rm BM}(x,\omega) = \pi U_{\rm BM}(x)/2\Delta\beta(x). \quad (13)$$

By conservation of fluid mass, the sum of the complex BM volume velocity $U_{\rm BM}(x)$ along the length of the cochlea and through the helicotrema *must* be equal to the volume velocity that enters the base of the cochlea $u_b S_0$, at any given stimulus frequency. This is more formally expressed as the volume sum

$$u_b S_0 = U(x_L) + \sum_{i=1}^{n_p} U_{\rm BM}(x_i), \quad (14)$$

where $U(x_L)$ is the volume velocity through the helicotrema and $x_i = \Delta i$. Note that $u_b S_0$ is a real quantity and thus the sum of the imaginary part of Eq. (14) must be zero. In the difference equation formulation of Allen (1977), Eq. (14) was found to be violated for low frequencies (below 200–300 Hz).This was true independent of the cochlear map used. We attribute this to an improper volume-velocity at the helicotrema boundary $U(x_L)$ in that model.

K. Summary

To this point we have formulated a one-dimensional cochlear model that includes scalae area variations, viscous losses due to perilymph, organ of Corti impedance variations etc., using the chain-matrix formalism. In the following we analyze the effects of variations in the cochlear map, scalae geometry, perilymph viscosity, and the helicotrema boundary conditions. The transmission line model was chosen so that each of these effects can be analyzed independently. Following Sondhi's observation that the cochlear input impedance for two-dimensional models is indistinguishable from that of one-dimensional models, we have assumed that the one-dimensional formulation will be adequate for this purpose.

III. RESULTS

A. Apical reflections and the cochlear map

As discussed in Appendix B, an important parameter for the computation of $Z_{\rm BM}(x)$ is the cochlear map. The cochlear map defines the BM peak velocity location along the length of the cochlea, as a function of the input frequency. The effect of three different *cat* cochlear maps on $Z_c(\omega)$ is compared in this section as follows. (1) Most existing cochlear models use a "straight" cochlear map of the form

$$f_{\rm CF}^{cs}(x) = 456[10^{(2.1/x_L)(x_L - x)}], \quad (15)$$

where x is the distance in cm from the stapes, the length of the cochlea is x_L, and CF stands for characteristic frequency. The c and s in the superscript stand for cat and straight cochlear map. (2) Liberman's (1982) cochlear map derived from single neuron labeling experiments is

$$f_{\rm CF}^{cl}(x) = 456[10^{(2.1/x_L)(x_L - x)} - 0.8]. \quad (16)$$

(3) Greenwood's (1961) cochlear map is derived from human psychophysical critical band experiments. It is then scaled from the human cochlea to the cat cochlea. The Greenwood cochlear map, with some modifications (Greenwood, 1990) to his original parameters, is

$$f_{\rm CF}^{cg}(x) = 456[10^{(2.1/x_L)(x_L - x)} - 1]. \quad (17)$$

It should be noted that the Greenwood cochlear map for the cat used here contains the original subtractive constant 1, whereas he now uses the constant 0.8 found by Liberman to provide the best fit to neural data (Greenwood, 1990). We have used a subtractive term of 1 simply to illustrate the effect of such a cochlear map on apical reflections.

These three cochlear maps are shown for comparison in Fig. 3. Once the cochlear map is chosen, our specification of $Z_{\rm BM}(x,\omega)$ is complete (see Appendix B).

Figure 4 shows $Z_c(\omega)$ corresponding to the three cochlear maps with an untapered cochlear model, zero viscosity, and a short-circuit helicotrema boundary condition. Figure 4(a) shows the magnitude of $Z_c(\omega)$ and Fig. 4(b) shows the phase of $Z_c(\omega)$. All succeeding figures illustrating impedance calculations will follow this format. The use of a straight cochlear map results in large oscillations in Z_c for input frequencies below $\approx$500 Hz, indicative of apical re-

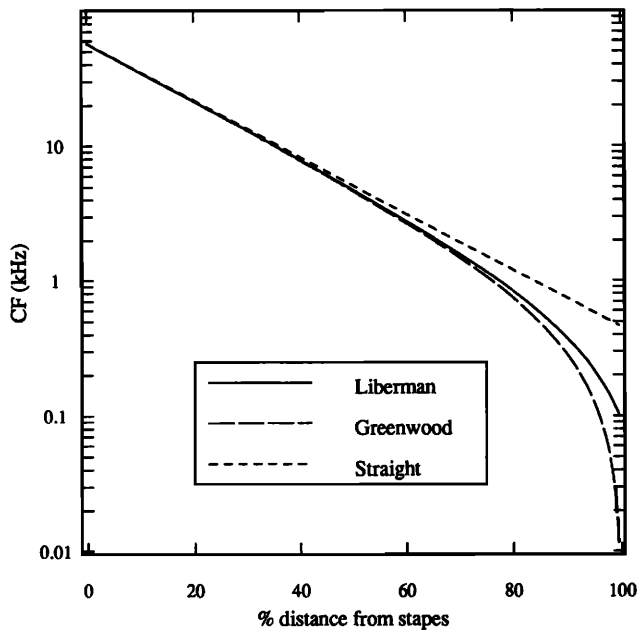

FIG. 3. Cochlear map functions for the cat anatomy pertaining to Eqs. (15)–(17) normalized to percent distance from the stapes. The difference between the three cochlear maps lies mostly in the frequency region below 1 kHz. The cochlear map is used in calculating the basilar membrane specific impedance $Z_{\rm BM}(x,\omega)$. Liberman's *cat* cochlear map $f_{\rm CF}^{cl}(x)$ based on single auditory-nerve fiber labeling experiments, will be used for all cat $Z_c(\omega)$ calculations in this study.

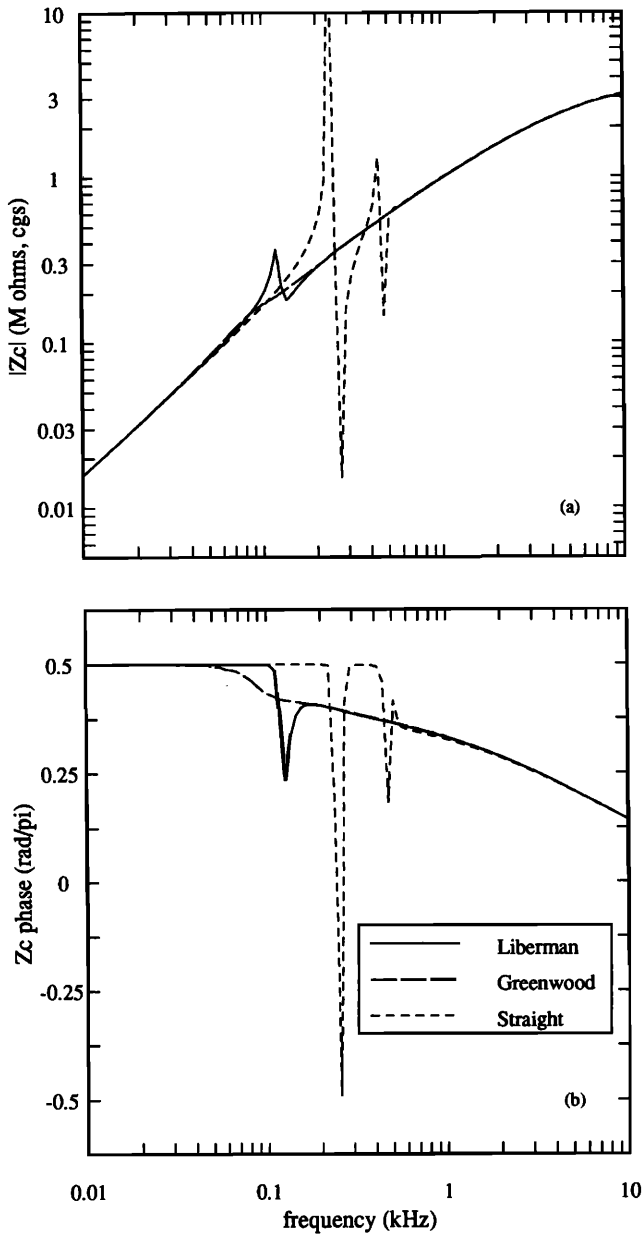

FIG. 4. Magnitude and phase of $Z_c(\omega)$ for each of the three cat cochlear maps of Fig. 3. The model parameters are: constant scalae area [$s(x) = 0.02\,\text{cm}^2$], no viscosity (NV, $\eta = 0$), and an acoustic short-circuit (SC) helicotrema boundary condition. The low-frequency limit of the straight cochlear map $f_{CF}^{cs}(x_L)$ is 456 Hz. Stimuli below this frequency result in large amplitude oscillation in Z_c indicating the presence of standing waves. The low-frequency limit of Liberman's cochlear map $f_{CF}^{cl}(x_L)$ is 91 Hz. In this case the amplitude of the apical reflections are significantly reduced, but nevertheless present for frequencies below $f_{CF}^{cl}(x_L)$. In Greenwood's cochlear map $\lim_{x \to x_L} f_{CF}^{cg}(x) \to 0$. In this case all frequencies are represented on the basilar membrane and thus the stimulus energy is dissipated by the motion of the BM before it reaches the apical end of the cochlea. Thus there are no apical reflections due to the end of the cochlear map when Greenwood's cat cochlear map is used. Standing waves exist when there are reflections at both the apical and at the stapes end of the cochlea. One way to eliminate the standing waves is to eliminate the apical reflections. Since the standing waves are eliminated by using Greenwood's cochlear map, we conclude that apical reflections are directly related to the low-frequency limit of the cochlear map $f_{CF}(x_L)$.

flections. Liberman's cochlear map reduces the apical reflections, and Greenwood's cochlear map virtually eliminates them.

To the best of our knowledge all previous cochlear models that have used the straight cochlear map have apical reflections, and therefore standing waves, for frequencies below 500 Hz. Published examples include the oscillations in the BM frequency response (Hubbard and Geisler, 1972; Matthews, 1980) as well as the presence of large oscillations in Z_c (Matthews, 1980), as shown in Fig. 4. Understanding and eliminating these artifacts is particularly important in time-domain implementations of nonlinear cochlear models.

Apical reflections are directly related to the low-frequency limit $f_{CF}(x_L)$ of the cochlear map. For example, close examination of Fig. 3 reveals that for f_{CF}^{cs}, frequencies below 456 Hz are not defined. Consequently, for input frequencies below this critical frequency, the traveling wave launched at the stapes will reach the apical end and be reflected back toward the stapes. This results in standing waves along the length of the cochlea; f_{CF}^{cl} does not define frequencies below 91 Hz and correspondingly there are apical reflections below 91 Hz. Note that the apical reflections actually begin at a frequency slightly above the low-frequency end of the cochlea because of the finite slope of the traveling wave apical to the CF.

In f_{CF}^{cg}, all frequencies of interest are represented and therefore there are no apical reflections. Only in the later case is the energy completely dissipated by the BM before the wave reaches the helicotrema. Minute reflections exist everywhere in the cochlea due to the stiffness gradient in the BM impedance (Viergever, 1988); however, these reflections have little effect on Z_c and may usually be ignored.

According to Greenwood, f_{CF}^{cg} was obtained by scaling the human function to the cat. Greenwood used a human-to-cat cochlea length ratio of 35:22, respectively. Cabezudo (1978) found the averaged cat cochlea length to be 2.36 ± 0.1 cm. Liberman found that the average cat cochlea length to be about 2.5 cm. Given this length, Liberman found the slope of the cochlear map to be the same as Greenwood's, but the end points of the cochlear map differed. Liberman derived a new cochlear map using the Greenwood formula, but with constants determined from his own data. Liberman's cochlear map f_{CF}^{cl} is based on intracellular labeling of single auditory-nerve fibers of known characteristic frequency, and is thus derived from a physical correlation between characteristic frequency and place. Unless otherwise stated, we will use f_{CF}^{cl} in all further calculations of the cat $Z_c(\omega)$.

B. Constant scalae area

Figure 5 shows the effects of viscosity and the helicotrema on $Z_c(\omega)$ for a constant scalae cross-sectional area cochlear model. The addition of viscosity has very little effect on Z_c except at frequencies below 50 Hz. Without perilymph viscosity (NV), a tube impedance (TI) helicotrema boundary condition slightly reduces the amplitude of apical reflections. The largest difference occurs near 25 Hz, where

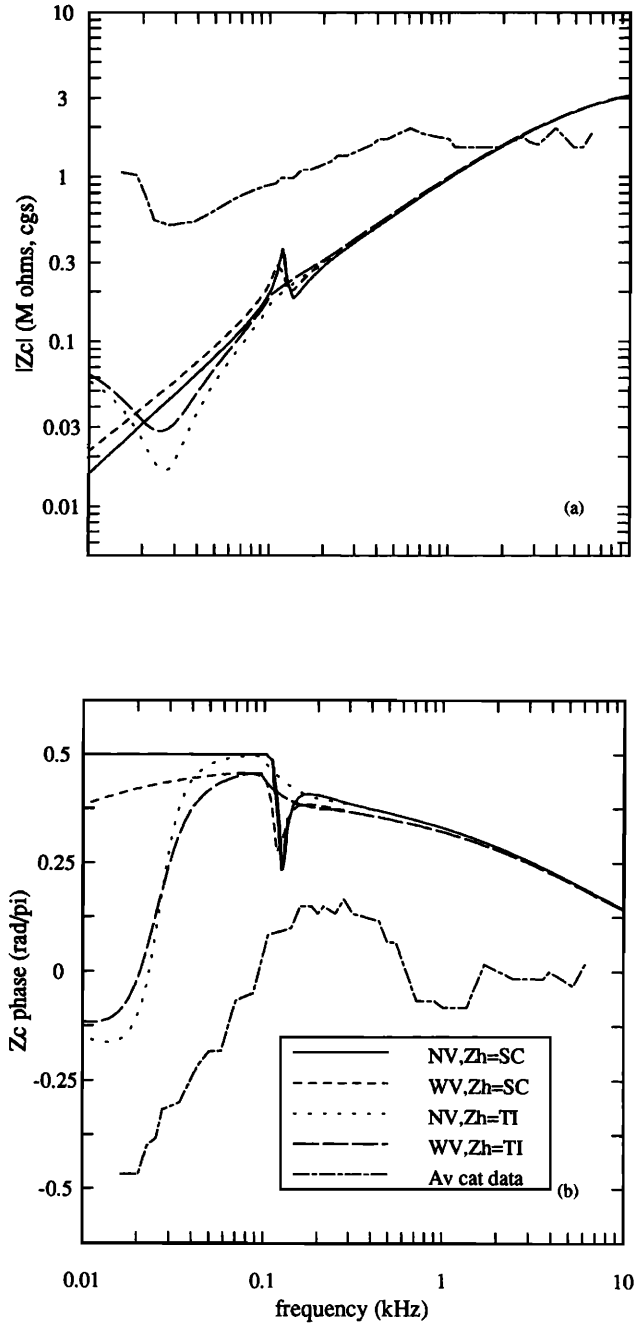

FIG. 5. The effects of the helicotrema and perilymph viscosity in a cochlear model with constant scalae area [$S(x) = 0.02\,\text{cm}^2$]. The "Av cat data" are the average cochlear input impedance of four cats by Lynch *et al.* (1982). The impedance measurements were made with the round window intact. The model calculations are without the round window. Model impedance calculations with perilymph viscosity (WV, $\eta = 0.02$) are not significantly different from the no viscosity (NV, $\eta = 0$) case. For a tube impedance (TI) helicotrema boundary condition, the magnitude of the cochlear input impedance tends to vary in the 25-Hz region, but it does not increase the impedance magnitude over a wide range of frequencies as is seen in the Lynch *et al.* data. The impedance magnitude does not increase when both a TI at the helicotrema and perilymph viscosity are included in the model. Thus the helicotrema, in terms of its effect on the magnitude of Z_c, is not as significant as that hypothesized by Dallos (1970). It is clear from the figure that the magnitude of model results and measured data diverge for frequencies below about 1 to 2 kHz, and the model phase is substantially higher (more masslike) than the phase of the averaged data.

$|Z_c|$ is reduced approximately by a factor of 2.5 (7.6 dB) and $\angle Z_c$ by approximately $-3\pi/4$. When perilymph viscosity is added (WV) to the TI case, $|Z_c|$ increases by approximately a factor of 1.6 (4.1 dB) near 25 Hz, and the phase changes by less than $\pi/18(10°)$ from the (NV,TI) case. Also shown in Fig. 5 is the average of cochlear input impedance measurements made on four cats by Lynch *et al.* (1982). The animal impedance measurements were made with the round window intact. Since the model computations were made without the round window, comparisons between data and model results are meaningful only for frequencies above ≈ 70 Hz. More will be said regarding the effects of the round window on cochlear input impedance in Sec. III E of the paper. Figure 5 indicates that the animal input impedance magnitude is higher than the magnitude of all four model cases for frequencies below about 1 to 2 kHz. The phase for all four model cases is significantly higher than the averaged phase data for all frequencies. *We conclude from Fig. 5 that in a constant scalae area model, neither the viscosity, or a realistic helicotrema, or the combination of the two, model the experimental data, which shows a significant increase in the cochlear input impedance magnitude below about 1 to 2 kHz.*

Dallos (1970) hypothesized a helicotrema consisting of a mass and damper in parallel with the cochlear structures, which is represented here as the TI boundary condition. Figure 5 shows that, for the constant scalae area model, Z_c is masslike in the 50-Hz $< f <$ 2-kHz region, independent of the helicotrema boundary condition. This conclusion seems to be in direct conflict with Dallos' hypothesis regarding the effect of the helicotrema on the cochlear input impedance.

C. Comparison of constant scalae area cochlear models

Some of the input impedance models from Table I that have constant scalae area and inviscid perilymph are plotted in Fig. 6. Not explicitly shown is Zwislocki's (1965, p. 37) theoretical consideration of the specific input impedance (Z_{cs}):

$$Z_{cs}(\omega) = (2\rho S_0 K_0/\beta_0)^{1/2} \times\{1 - j[\omega R_m C + (R/\omega\rho)]\}^{-1/2}. \quad (18)$$

By assuming the curly-braced quantity of Eq. (18) to be approximately equal to 1, Zwislocki concludes that "the specific input impedance of the cochlea is independent of frequency and is real." Note that the left-hand term of Eq. (18), when divided by S_0, is equivalent to the radiation resistance R_c derived from the WKB solution (Allen, 1979), which is equal to $2\rho c_0/S_0$, where c_0 is the velocity of the traveling wave on the BM.

Dallos (1973, Fig. 4.15) calculated Eq. (18) exactly and showed that Z_{cs} is resistive at frequencies above ≈ 30 Hz—for a given set of parameters. In Dallos' helicotrema model of Z_c, the impedance due to the cochlea Z_{cs} is taken to be independent of frequency; i.e., $Z_{cs} = R_c$.

The solutions for Z_c by the WKB method and Koshigoe *et al.*'s [1983, Eq. (62) without K_{rw}] are also shown in Fig. 6. As a result of approximations in their formulation, Koshigoe *et al.*'s constant scalae area results are valid only in the

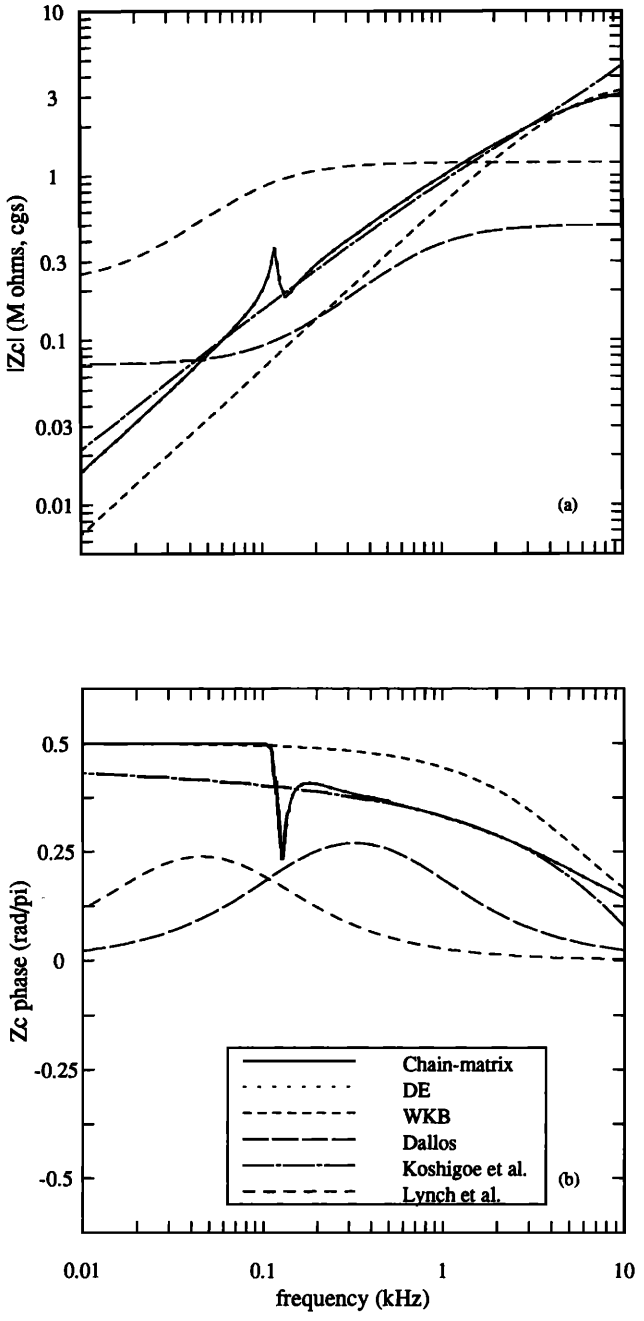

FIG. 6. Comparison of previous models of Z_c having constant scalae area and inviscid perilymph (see also Table I). As a verification of the chain-matrix calculations, a one-dimensional transmission line model of the cochlea was computed by the difference equation (DE) method using the same set of parameters; the two curves are indistinguishable from each other. The Lynch *et al.* phenomenological model indicates that Z_c is resistive at frequencies above $\approx$400 Hz. The theoretical models indicate a masslike behavior at these frequencies. Dallos' model resembles the Lynch *et al.* model but the physiological mechanisms attributed to Dallos' helicotrema model of $Z_c(\omega)$ is not consistent with our results (see Fig. 5). Also shown are the constant scalae area closed-form expressions of Z_c by Koshigoe *et al.* (1983), valid for frequencies below approximately 1 kHz, and the WKB solution (Allen, 1979), valid for frequencies above approximately 1 kHz. This figure shows that the constant scalae area model calculations using the chain matrix can be approximated by Koshigoe *et al.*'s (1983) constant scalae area model for frequencies below approximately 4 kHz and by the WKB solutions (Allen, 1979) for frequencies above approximately 4 kHz.

30-Hz–1-kHz frequency region (Koshigoe *et al.*, 1983, p. 489). Both Koshigoe *et al.* and the WKB results are derived under the assumption that there is only a forward traveling wave. Since the chain-matrix method for a constant scalae area yields a result similar to that of Koshigoe *et al.*, we might reasonably conclude that: (a) the two results give the same answer over most of the frequency range, and (b) reflections along the cochlea can be ignored above $f_{CF}(x_L)$, which for Liberman's cochlear map is 91 Hz.

Figure 6 shows that in the Koshigoe *et al.*, WKB, and chain-matrix constant scalae area model results are not in agreement with the Lynch *et al.* model based on averaged data. For example, at 70 Hz $|Z_c|$ of the theoretical models are below Lynch *et al.*'s model by a factor of more than 6 (15.6 dB). The model phase is $\pi/3$ larger than the experimental data (in Koshigoe *et al.*'s calculations, the discrepancy in phase is somewhat less).

All models considered thus far have been one-dimensional models, and the possibility remains that in two-dimensional, or even three-dimensional models, the theory and experimental results would agree. Higher dimensional models might be expected to effect the results at higher frequencies where the wavelength is shorter. Sondhi (1978) has shown that, for specific model parameters and with constant scalae area and zero viscosity, the acoustic input impedance of a two-dimensional and a one-dimensional model is identical. Therefore, a higher dimensional model does not appear to help. Finally, experimental observations indicate that pressure in the scala vestibule, near the base, is relatively independent of depth of the measurement probe into the vestibule in the frequency range below 10 kHz (Nedzelnitsky, 1980).

In summary, for constant scalae area and no viscosity, the best approximation to the exact calculations by our chain-matrix methods is Koshigoe et al.'s for 30 Hz $< f <$ 4 kHz and WKB for $f >$ 4 kHz. The parameters considered thus far, namely, viscosity, helicotrema, cochlear map, and dimensionality of the model, do not appear to close the gap between theory and measurements.

D. Effects of tapered scalae area

The geometry of the scalae is not that of a constant cross-sectional scalae area as has been assumed thus far. Wever (1949) and Dallos (1970) have made anatomical measurements of the scalae cross-sectional area. To a first-order approximation Dallos found the scala vestibule area to be exponentially decreasing along the length of the cochlea [i.e., $S(x) = S_0 \exp(-s_1 x)$]. Here, S_0 is the area at the base and $s_1 \geqslant 0$ is the rate of change parameters of the area. In this section we consider the effects of the parameters S_0 and s_1 on $Z_c(\omega)$. In addition, we also analyze the interaction of these parameters with viscosity and the helicotrema boundary condition.

1. Inviscid perilymph

Figure 7 shows $Z_c(\omega)$ in a cochlea without perilymph viscosity ($\eta = 0$) and Liberman's cochlear map, as a func-

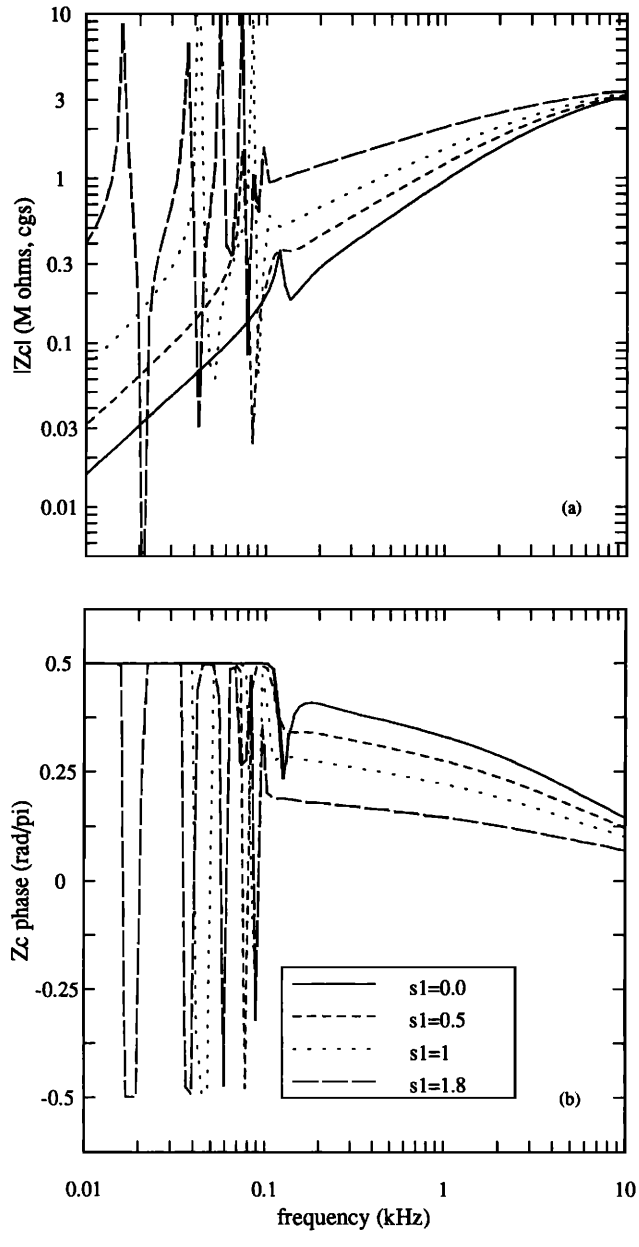

FIG. 7. The effect of tapering in a cochlear model with inviscid perilymph ($S_0 = 0.02\ \text{cm}^2$, Z_h = SC). This figure shows that Z_c is strongly dependent on the change in the scalae area. For stimulus frequencies greater than $f_{\text{CF}}^{\text{cl}}(x_L)$, as the tapering parameter s_1 (cm^{-1}) increases, $|Z_c|$ increases, and $\angle Z_c$ decreases. This indicates that, above this frequency, the real part of Z_c increases as tapering increases. In addition, as tapering increases, the amplitude of the apical reflection also increases for stimulus frequencies below $f_{\text{CF}}^{\text{cl}}(x_L)$. This is due to an increase in impedance mismatch between the helicotrema and the scalae, at the end of the cochlea.

tion of the taper parameter s_1. The following observations are made.

(a) There is an overall increase in $|Z_c|$ as tapering increases. For frequencies above $f_{\text{CF}}^{\text{cl}}(x_L)$, the $\angle Z_c$ decreases as tapering increases, which means that tapering makes the cochlea more resistive. Equation (A1) shows that the series impedance increases as the area decreases. Thus, for a fixed S_0, as the tapering parameter increases so does the series impedance. Shera and Zweig (1990) have recently hypothesized that the increasingly resistive behavior of Z_c, with an increase in tapering parameter s_1, is due to an increase in cancellation of the mass dominated series impedance $Z'(x,\omega)$ and the compliance dominated shunt admittance $Y'(x,\omega)$, basal to the characteristic place.

(b) As tapering increases, the amplitude of the standing waves seen in Z_c increase dramatically for frequencies below $\approx f_{\text{CF}}^{\text{cl}}$. As mentioned above as s_1 increases so does the series impedance and this results in a larger reflection coefficient at the apical end of the cochlea, leading to an increase in the standing wave amplitude.

(c) For frequencies below $f_{\text{CF}}^{\text{cl}}(x_L)$, Fig. 7(b) indicates that Z_c is largely mass dominated.

2. Viscous perilymph

Figure 8 shows the same parameter range for s_1 as Fig. 7, but with the perilymph viscosity set to the normal value of $\eta = 0.02$. By comparison with Fig. 7, we make the following conclusions.

(a) For frequencies greater than ≈ 150 Hz, $|Z_c|$ increases as s_1 increases and is within 1 dB of $|Z_c|$ for the no viscosity case, with the corresponding $\angle Z_c$ being within 0.05 π (9°) of the no viscosity case. Thus viscosity has only a small effect on the impedance for frequencies greater than ≈ 150 Hz.

(b) For frequencies greater than ≈ 150 Hz, Z_c becomes increasingly real as tapering parameter (s_1) increases.

(c) For frequencies below ≈ 150 Hz, Z_c becomes more resistive as tapering parameter s_1 increases only for the viscous perilymph case. Therefore, viscosity becomes increasingly important as the scalae radius in the apical region becomes comparable to the viscous boundary layer thickness [see Eq. (A4)].

(d) As tapering is increasing, oscillations in Z_c due to the end of the cochlear map $f_{\text{CF}}^{\text{cl}}(x_L)$ are diminishing for the viscous case; in fact, there are no oscillations in Z_c for $s_1 = 1.8$. Therefore, the viscous boundary layer dissipates the apical reflections.

(e) If tapering is increased beyond a certain point for the viscous case, then phase of Z_c may become negative, indicating a compliant behavior. For example, for $s_1 = 1.8$ (arbitrarily chosen), the phase is negative for frequencies below 60 Hz. Our interpretation of this observation is that the increase in tapering results in the scalae impedance being greater than the BM impedance. Thus it is easier for the perilymph to flow "into" the BM than to flow down the scala vestibule.

In the above discussions of Figs. 7 and 8, there are two important frequencies. First, apical reflections occur due to the cochlear map limit. This frequency will be referred to as $f_{\text{CF}}(x_L)$. Second, viscous effects become important when the viscous boundary layer becomes comparable to scalae radius. The frequency where this occurs depends on the scalae radius in the apical region. For a fixed S_0 (as in Figs. 7 and 8), the scalae radius depends on the tapering parameter s_1. The viscous boundary layer thickness is frequency depen-

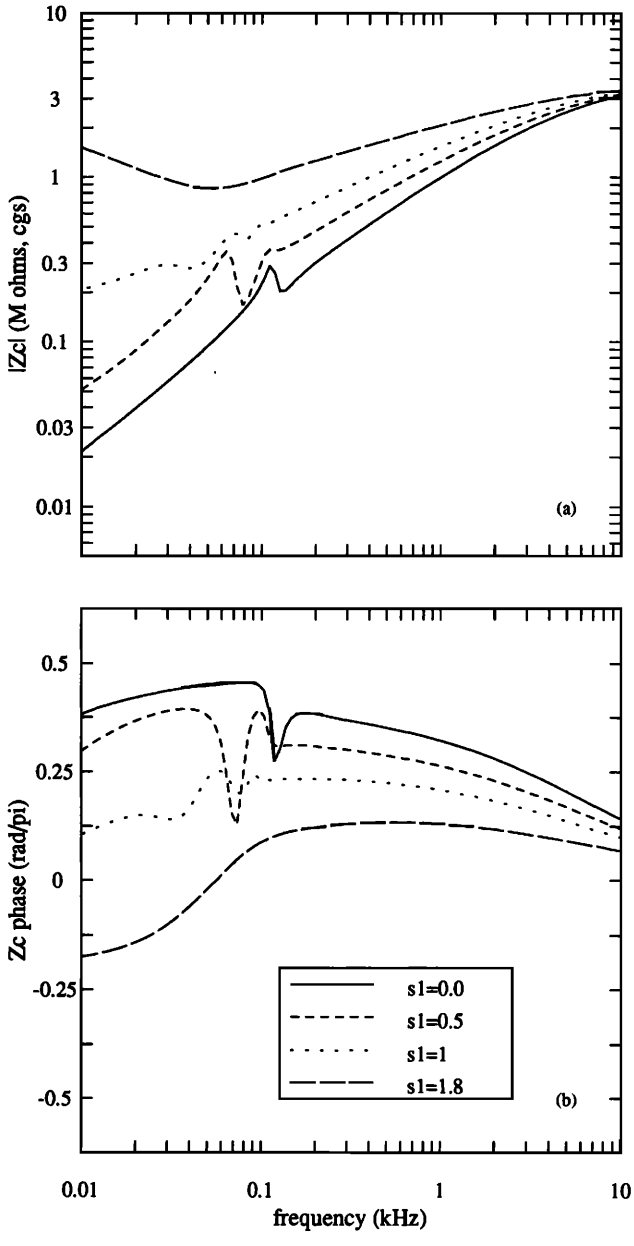

FIG. 8. The effect of tapering in a cochlear model with viscous perilymph ($\eta = 0.02$, $S_0 = 0.02$ cm^2, Z_h = SC): Above approximately 150 Hz, Z_c is similar to the no viscosity case (Fig. 7). Below that frequency, Z_c becomes more and more resistance dominated as tapering increases. As tapering increases, the tube radius in the apical region becomes more comparable to the viscous boundary layer thickness. Thus we conclude that interaction of the reduced radius in the apical region with the viscous perilymph gives rise to R_0 in the Lynch *et al.* model. In addition, as tapering is increasing, apical reflection due to the low-frequency limit of the cochlear map are diminishing. Thus the presence of viscosity dissipates the apical reflections by a significant amount.

dent and is proportional to $1/\sqrt{f}$ (see Appendix A). Thus, for a given tapering parameter s_1, the cochlear input impedance will become more and more resistive as the frequency decreases.

If we define f_{bl} to be the frequency at which the viscous boundary layer becomes equal to the tube radius, then, by setting $r_v = 1$ in Eq. (A3), we obtain $f_{bl} = 0.5\eta\rho^{-1}S^{-1}(x)$. For $S_0 = 0.0175$ and $s_1 = 1.3$, f_{bl} is 15 Hz at $x = x_L$. Thus, near 15 Hz, the viscous effects completely dominate. However, viscosity will start to have an effect at frequencies greater than 15 Hz. For the purposes of discussion, we have chosen 150 Hz as the frequency below which viscous effects become important. Coincidentally, this frequency is close to $f_{CF}^{cl}(x_L)$. This frequency was chosen based on when Z_c was more real rather than mass dominated. For these parameters, r_v the ratio of tube radius to viscous boundary layer is approximately 2.46. If one were to recompute the calculations of Fig. 8 with f_{CF}^{cg}, then the effects of viscosity below 150 Hz on Z_c would still be observed, but without the complications of reflections below $f_{CF}^{cl}(x_L)$.

Figure 9 shows how $|Z_c|$ scales with S_0 for a fixed $s_1 = 1.0$, and with $\eta = 0.02$. The overall shape of $|Z_c|$ is maintained with no significant change in the slope of $|Z_c|$ for each value of S_0. For frequencies above $\approx f_{CF}^{cl}(x_L)$, $|Z_c| \propto S_0^{-\nu}$ and $\angle Z_c$ is, to a first-order approximation, independent of S_0. For large S_0, ν is a weak function of S_0. But, for $S_0 < 0.03$ cm^2, ν is constant and is ≈ 0.87. Thus, given Z_c at one frequency and the corresponding S_0, one can evaluate the proportionality constant and therefore find $|Z_c|$ for any other S_0 at that frequency.

3. Effects of the helicotrema with tapering

In Sec. III B the effects of the helicotrema boundary condition for a constant scalae area model were analyzed. In a similar manner we now analyze the effect of the helicotrema in the tapered cochlear model. In Fig. 10 four possibilities are considered: with and without viscosity (WV,NV), and using two different helicotrema boundary conditions (SC,TI). This gives a four-way comparison. By comparison of Fig. 7 to Fig. 8, we showed that the introduction of viscosity greatly reduces the low-frequency standing waves in a tapered cochlea. Figure 10 shows that changing the helicotrema boundary condition from SC to TI, in the zero viscosity case, has the effect of reducing the magnitude of the oscillation in Z_c, but its effect is not as great as that due to viscosity alone. In addition, for frequencies below ≈ 150 Hz, Z_c is resistance dominated in the viscous perilymph case and it is mass dominated when perilymph viscosity is zero. Introducing a TI boundary condition when perilymph viscosity is already present has little effect on Z_c. *We therefore conclude that in the tapered cochlea, the effects due to the viscous perilymph are more significant than the effects due to the acoustic impedance of the helicotrema.* Unless otherwise stated, all further calculations of Z_c will be assumed to be with $\eta = 0.02$ and Z_h = SC.

E. Comparison of tapered scalae area cochlear models

The Koshigoe *et al.* model is the only model in Table I that includes the effect of tapering. But, as they stated in their paper: "In our approximate analysis, apical reflections are ignored" (Koshigoe *et al.*, 1983, p. 488). Thus their ana-

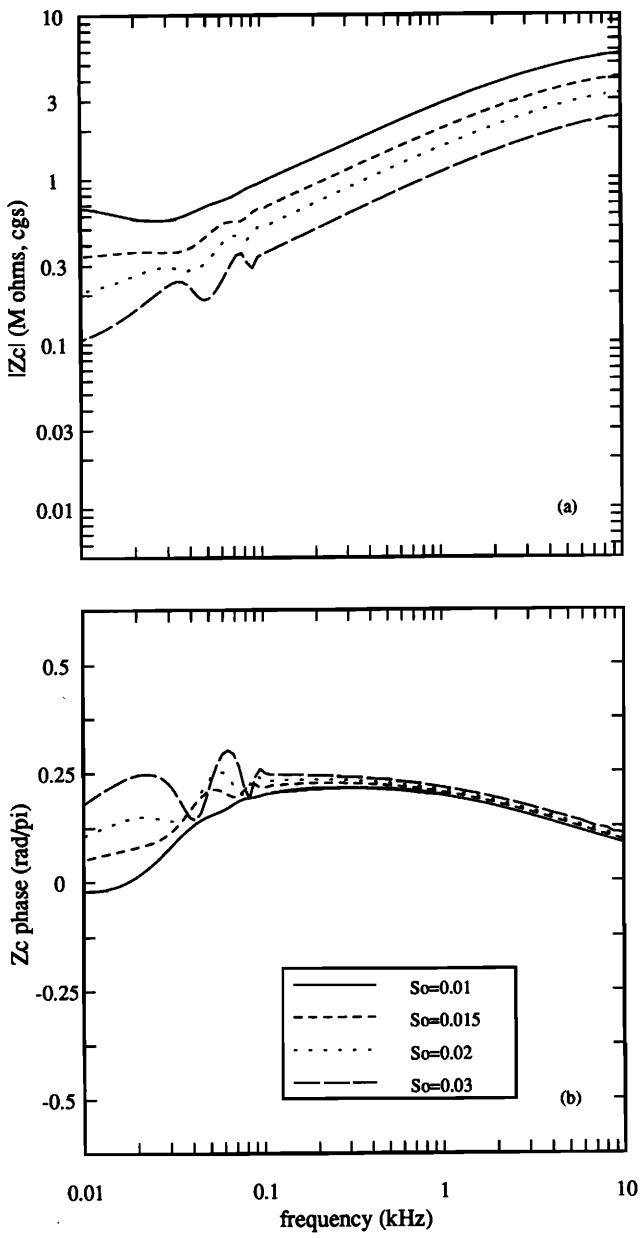

FIG. 9. The effect of S_0 in a cochlear model with tapering parameter s_1 fixed ($s_1 = 1.0$, $Z_h = \mathrm{SC}$). For frequencies above $\approx f_{\mathrm{CF}}(x_L)$, scaling $S(x)$ (i.e., by decreasing S_0) effectively results in a proportional translation in $|Z_c|$ with only a small effect on $\angle Z_c$. For this case $|Z_c| \propto S_0^{-\nu}$, where $\nu \approx 0.87$ (see text).

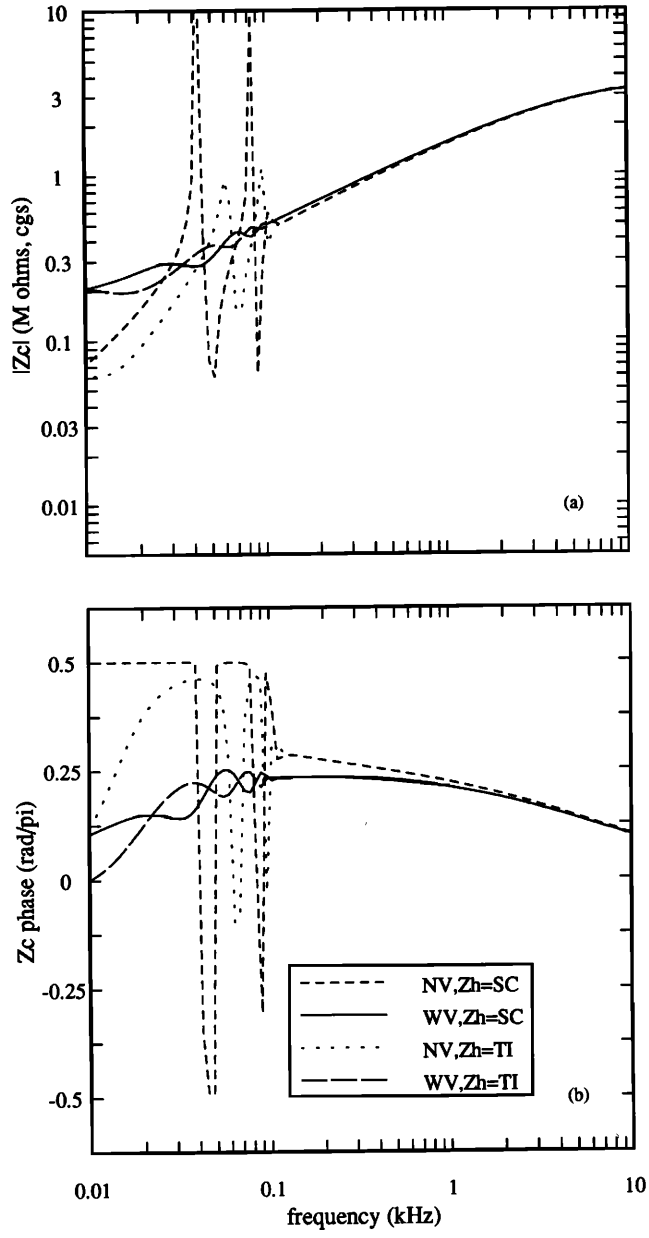

FIG. 10. The effects of the helicotrema and perilymph viscosity in a tapered cochlear model ($S_0 = 0.02$, $x_1 = 1.0$). As shown here, and in Figs. 7 and 8 the introduction of viscosity (WV) virtually eliminates the apical reflections that result in the standing waves. A tube impedance (TI), in the no viscosity case, reduces the apical reflections but its effect is not nearly as great as that due to viscosity alone. For frequencies less than approximately 150 Hz, the phase indicates that Z_c is resistance dominated only when viscosity is present. Thus, when tapering *and* viscosity are present, a TI model of the helicotrema has a negligible effect.

lytic method does not lend itself to the type of analysis we have established in the previous sections where apical reflections can be of considerable importance.

Figure 11 compares, for the same set of parameters, our results for the acoustic input impedance with those of Koshigoe *et al.*'s numerical calculations. In this figure only, K_0' was adjusted to match K_0 used by Koshigoe *et al.* Measured data and Koshigoe *et al.*'s numerical calculations assume a round window stiffness K_{rw}. The round window impedance $Z_{\mathrm{rw}}(\omega) = K_{\mathrm{rw}}/s$ adds to the cochlear input impedance as a series impedance (Nedzelnitsky, 1980):

$$Z_{\mathrm{crw}}(\omega) = K_{\mathrm{rw}}/s + Z_c(\omega). \tag{19}$$

Nedzelnitsky (1980) concluded that the effect of the round window, in the cat, is important for frequencies below ≈ 300 Hz. To fit $|Z_c|$ for frequencies below 40 Hz, where $Z_c \cong Z_{\mathrm{rw}}$,

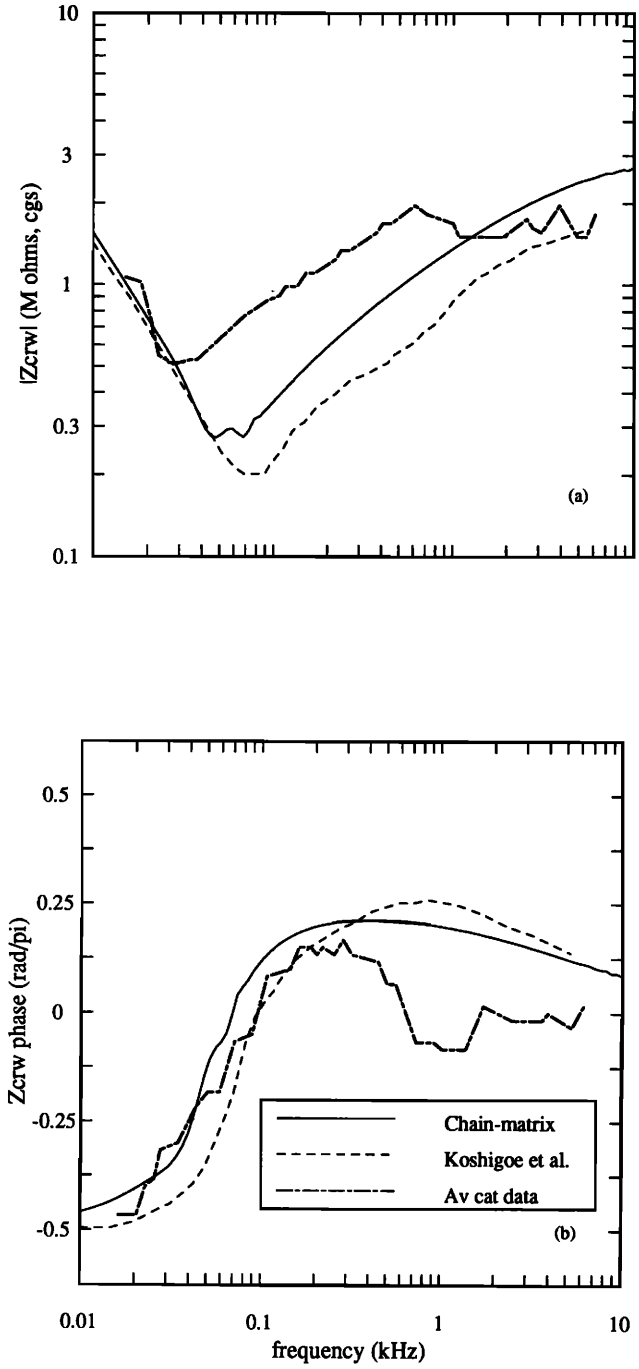

FIG. 11. Comparisons of measured data and cochlear models with tapered scalae area. The impedance of the round window $Z_{rw}(\omega)$ has now been added to the model calculations of $Z_c(\omega)$. The sum of these impedances is referred to as $Z_{crw}(\omega)$. Koshigoe *et al.*'s numerical results (their analytical approximations) are from their Figs. 1 and 2. Parameters for both models are: $S_0 = 0.02$, $s_1 = 1$, $K_0' = 10^9$, $\eta = 0.02$, Z_h = SC, and the round window stiffness K_{rw} is 10^8. In the chain-matrix model, Liberman's cochlear map was used. In Koshigoe *et al.*'s calculations, an exponential stiffness was assumed. "Av cat data" are from Lynch *et al.* (1982). Although the chain-matrix calculations are in better agreement with the data than the Koshigoe *et al.*, calculations, discrepancies still exist. For example, for frequencies above 500 Hz, the discrepancy in phase is as large as $\frac{1}{3}\pi$ (60°) and, for frequencies below 1 kHz, the discrepancy in magnitude is as large as a factor of 2.5 (8 dB) (note the change in magnitude scale from previous figures).

Lynch *et al.* (1982) chose a value of 10^8 dyn/cm^5 for the round window stiffness. Unless otherwise stated, we will use this value for the round window stiffness. This value of the round window stiffness has an effect on the phase for frequencies up to 70 Hz. Thus, when referring to effects above 70 Hz, we will use Z_c and Z_{crw} interchangeably. Unless otherwise stated, all further calculations in this section will include K_{rw}.

From Fig. 11, despite a similar choice of parameters, the chain-matrix model and Koshigoe *et al.*'s model show a ratio of up to 1.7 (4.6 dB) between 0.1 and 8 kHz. The most obvious explanation for the differences between our and Koshigoe *et al.*'s results is that the Koshigoe *et al.* solution is an approximate solution, while our chain-matrix solution is an exact numerical solution. This approximation has two parts. The *first* is that our numerical solution includes a forward and backward traveling wave, whereas Koshigoe *et al.*'s method includes only a forward traveling wave. Specifically, the Koshigoe *et al.* model ignores reflections due to scalae tapering and apical reflections. *Second* is the approximations for the series impedance they make in finding the solutions.

There is also a significant difference between the conclusions arrived at by the chain-matrix method and those of Koshigoe *et al.* For frequencies above $\approx$150 Hz, we have presented evidence that the low-frequencies increase in $|Z_c|$ is independent of viscosity and is due only to tapering. For frequencies below $\approx$150 Hz, the phase indicates that Z_c is resistance dominated due to presence of *both* viscosity and tapering, independent of the helicotrema impedance. Koshigoe *et al.*, on the other hand, argue that it is viscosity alone that is responsible for the rise in $|Z_c|$ below 500 Hz.

F. Comparison with measured data

Figure 11 compares averaged Z_{crw} obtained by scala vestibule pressure and stapes velocity measurements in anesthetized cats (Lynch *et al.*, 1982) with our model calculations of Z_{crw} (in Lynch *et al.*, Z_{crw} is referred to as Z_c). There is some agreement in $|Z_{crw}|$ for frequencies above 2 kHz but poor agreement in $\angle Z_{crw}$ above 500 Hz. For frequencies below 200 Hz, our theoretical calculations match measured $\angle Z_{crw}$ quite well. But our model $|Z_{crw}|$ is below the average data by as much as a factor of 2.5 (8 dB) in the frequency region between 30 Hz and 1 kHz. Lynch *et al.* estimate their experimental worst-case error to be $\pm$ 10 dB; however, the "actual measurement errors are likely to be substantially smaller than these worst-case estimates of error *limits*" (Lynch *et al.*, 1982, p. 113). Shera and Zweig (1990) have recently made minimum-phase fits to the amplitude and phase of the Lynch *et al.* data. Their calculations indicate that the data stays minimum phase for approximate deviations of $\pm$ 2 dB in amplitude and $\pm$ 10° in phase. Thus, although the measurement errors are not exactly known we assume that they are sufficiently small. This indicates that the parameters chosen to calculate our model results need to be reevaluated.

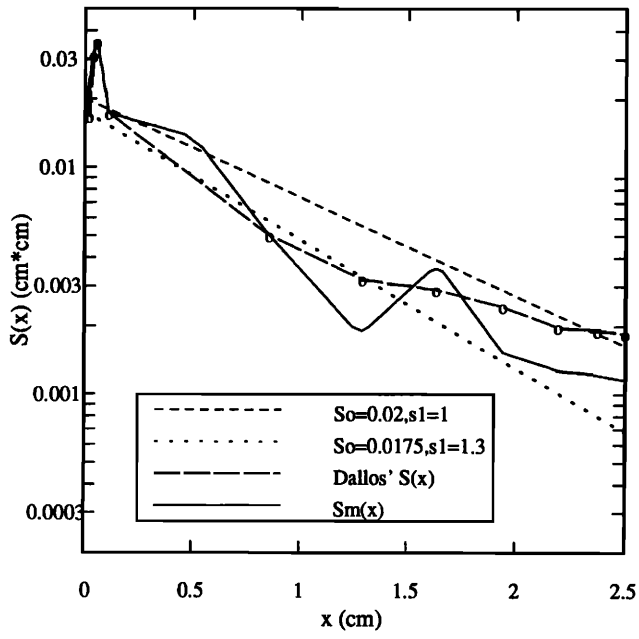

FIG. 12. Anatomical measurements of cat scala vestibule area $S(x)$. The basal end corresponds to $x = 0$ and the apical end of the cochlea corresponds to $x = 2.5$ cm. The circles indicate anatomical measurements in one cat (Dallos, 1970). The curve with $S_0 = 0.02$, $s_1 = 1$ is an approximate fit to the measured area function (Dallos, 1970). The curve with $S_0 = 0.0175$, $s_1 = 1.3$ is another approximate fit to the measured area function, $S_m(x)$ is Dallos' area function heuristically modified (see text) to obtain a better fit to measured $Z_{crw}(\omega)$.

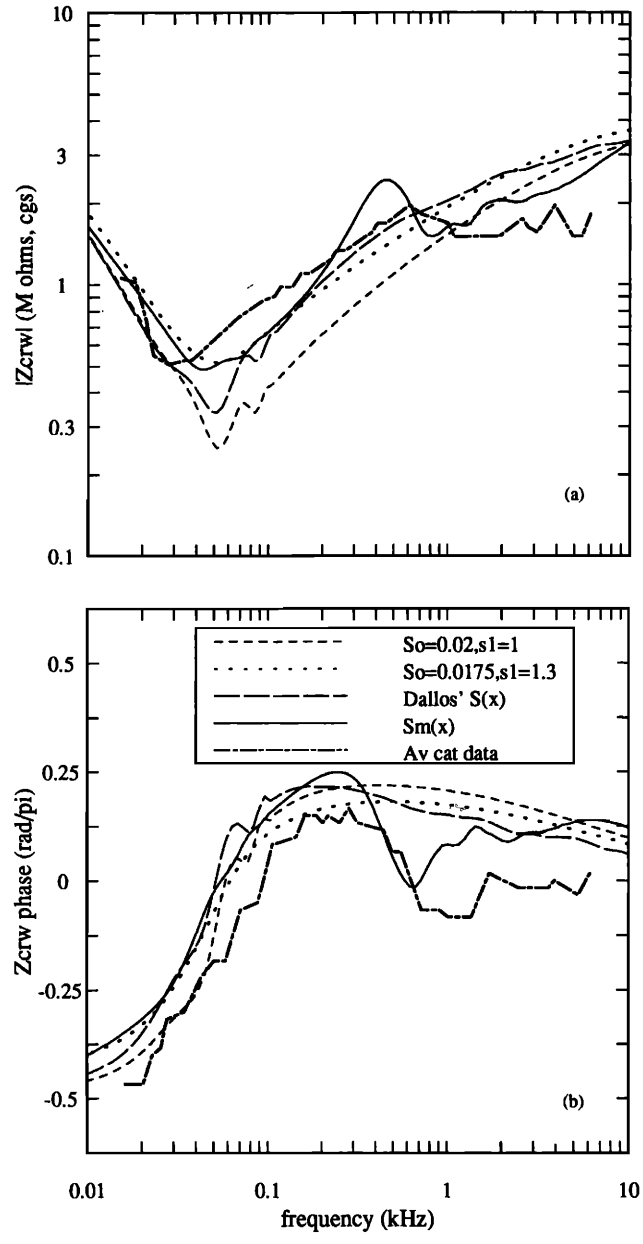

FIG. 13. $Z_{crw}(\omega)$ corresponding to the area functions of Fig. 12. Going from the $S_0 = 0.02$, $s_1 = 1$ curve to the $S_0 = 0.0175$, $s_1 = 1.3$ curve results in a better agreement between the calculated $Z_{crw}(\omega)$ and the measured data. Using the actual measured area function of Dallos yields only a slight improvement. When Dallos' area function is heuristically modified as in $S_m(x)$ of Fig. 12, then there is a better agreement between the calculated $Z_{crw}(\omega)$ and the measured data. The decrease in phase near 300 Hz is due to the local maximum in the area function $S_m(x)$ apical to $x = 0.9$ cm. $K_{rw} = 10^8$ (Lynch *et al.*, 1982) for all four cases.

1. The appropriate geometric representation

As mentioned previously, the most important parameter that affects the cochlear input impedance is the scalae area function. Thus, in this section, we further explore the effect of $S(x)$ on $Z_c(\omega)$. Figure 12 shows the various area functions that we use next to calculate $Z_c(\omega)$. To our knowledge, the only anatomical measurement of the area function for the cat scala vestibule is one by Dallos (1970). The $S_0 = 0.02$ cm^2 and $s_1 = 1$ cm^{-1} curve is the approximate fit made by Dallos to the measured area function; this is the approximation that we have used to this point. The $S_0 = 0.0175$ cm^2 and $s_1 = 1.3$ cm^{-1} curve is a second approximation to the measured area function. Discussion of the $S_m(x)$ curve is deferred for the moment. The effect of each of these area functions on $Z_c(\omega)$ is shown in Fig. 13.

For frequencies below 1 kHz, we see that a better fit to $|Z_{crw}|$ is obtained with $S_0 = 0.0175$ cm^2 and $s_1 = 1.3$ cm^{-1} than with $S_0 = 0.02$ cm^2 and $s_1 = 1$ cm^{-1}. However, even with this area function, our match to averaged phase is still poor for frequencies above 400 Hz. In the experimental data, the phase starts to decrease near 300 Hz becoming negative near 500 Hz, and it stays negative for frequencies up to 2 kHz. Above 2 kHz, the phase is approximately zero, indicating that Z_c is more or less resistive. The model Z_{crw}, on the other hand, approaches zero phase gradually, still having an angle of $\pi/10$ rad at 10 kHz. Near 5 kHz there is also a systematic error in $|Z_c|$, becoming as large as 1.8 (5.1 dB) at high frequencies. Since we have shown that the geometry of the cochlea has an important effect on Z_c, perhaps representing $S(x)$ by an exponentially tapered function is not a sufficient approximation for the purposes of accurately calculating the input impedance. Figure 13 shows calculations

of Z_{crw} using Dallos' measured area function of the scala vestibule, which results in an input impedance that is not significantly different from the one obtained with $S_0 = 0.0175$ and $s_1 = 1.3$. Therefore, the errors as stated above persist.

The scala vestibule area measured by Dallos is for one cat only. In addition, an error bound on the measurement was not provided by Dallos. To better fit the average cochlear input impedance data, we have tried slight perturbations (less than a factor of 2) to the measured area function. In the apical region, the $S_0 = 0.0175$ and $s_1 = 1.3$ curve has a smaller area than the $S_0 = 0.02$ and $s_1 = 1$ curve. Since the former area function results in a better fit, we have decreased the measured area in the region apical to 0.9 cm; with the exception of the 1.6-cm region, where the area was slightly increased. Figure 12 shows that the net effect of these changes results in an area function with a local maximum in the apical region of the cochlea. One important motivation for making these changes comes from the observation that the scalae vestibule area function measurements are not monotonically decreasing in the human cochleas (Wever, 1949, pp. 276–278) (see Fig. 16). Figure 13 shows that this local increase in the area function gives rise to a sharp decrease in phase above approximately 300 Hz. From Fig. 12 we note that there are no area measurements in the $0.1 < x < 0.85$-cm region. Perhaps the area function in this region cannot be approximated by an exponential function as we have assumed. Based on our experience with perturbation of the area at the $x = 0.5$-cm point, we have increased the scalae area by a factor of 1.5 at that point. The result of increasing the area near the $x = 0.5$-cm region is to decrease the magnitude and phase of Z_c above the 3- to 4-kHz region, which is consistent with the measured Z_c data. The area function with the modifications described above is referred to as $S_m(x)$ in Fig. 12. The input impedance corresponding to $S_m(x)$ is shown in Fig. 13. *The resulting cochlear input impedance calculations are in very close agreement with those of the averaged measured data.*

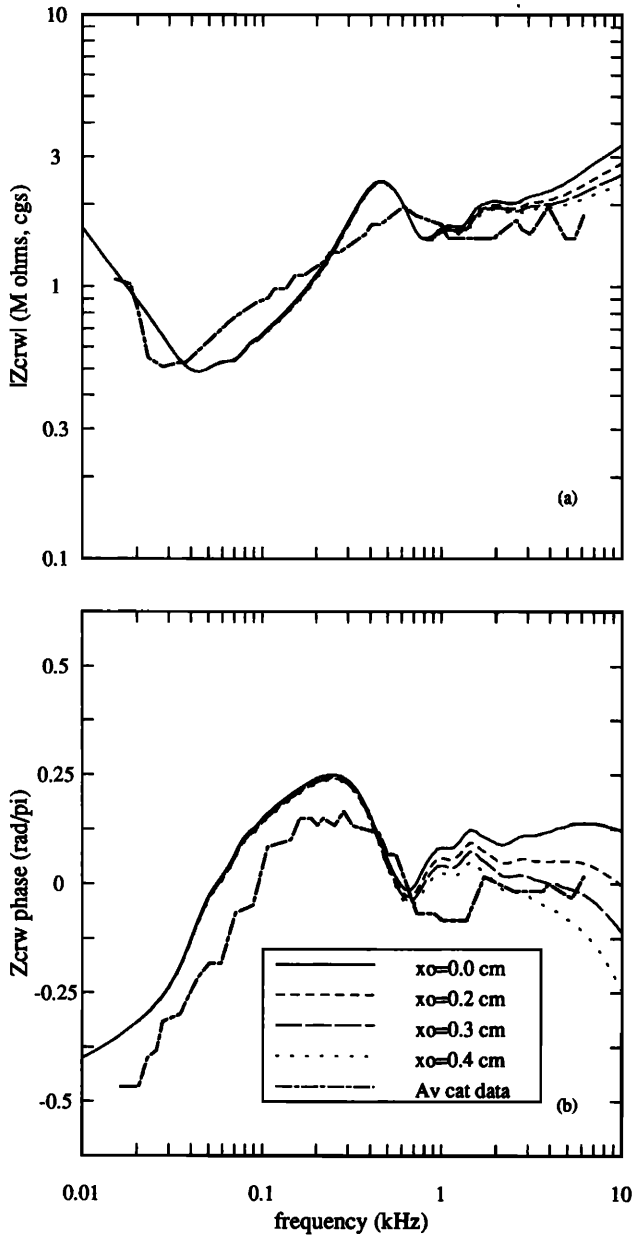

FIG. 14. The effect on $Z_{crw}(\omega)$ of placing the pressure transducer at distances x_0 apical to the stapes. The major effect of placing the pressure transducer at different location along the length of the cochlea is in the phase $[S(x) = S_m(x)]$.

2. Effect of transducer placement

In calculating the load to the middle ear, one should use the pressure in the scala vestibule at the stapes—as we have done thus far. However, for comparison to measured Z_c data, one should use the pressure inside the scala vestibule in the vicinity of the transducer. Thus we need to know the location of the transducer relative to the stapes. Figure 14 shows the results of evaluating Eq. (10) at various locations near the stapes; i.e., use $P(x_0)$ instead of $P(0)$. For frequencies below 1 kHz, there are virtually no differences in $|Z_{crw}|$ and $\angle Z_{crw}$ as a function of x_0, which we define as the distance from the stapes. But for frequencies above 1 kHz, large differences in $\angle Z_{crw}$ exist as a function of x_0. Figure 14 shows that the phase decreases with an increase in x_0. Individual cat data (Lynch *et al.*, 1982) in Fig. 15 display negative phase for some of the high-frequency data points. A change in x_0 is one model parameter that results in a negative phase above 2 kHz. This distance is most likely to be difficult to measure experimentally, and was not reported by Lynch *et al.* (1982). However, Fig. 2 of Lynch *et al.* (1982) suggests that $x_0 < 0.2$ cm. To calculate the model result shown in Fig. 15, we have chosen $x_0 = 0.15$ cm.

G. Interanimal comparison with the chain-matrix model

Up to now, we have been using the Lynch *et al.* averaged Z_c data. The parameters used thus far have proven to capture some of the detail present in the averaged Z_c data. Since averaging of data smears out details, we now wish to compare our results with the individual measurements from

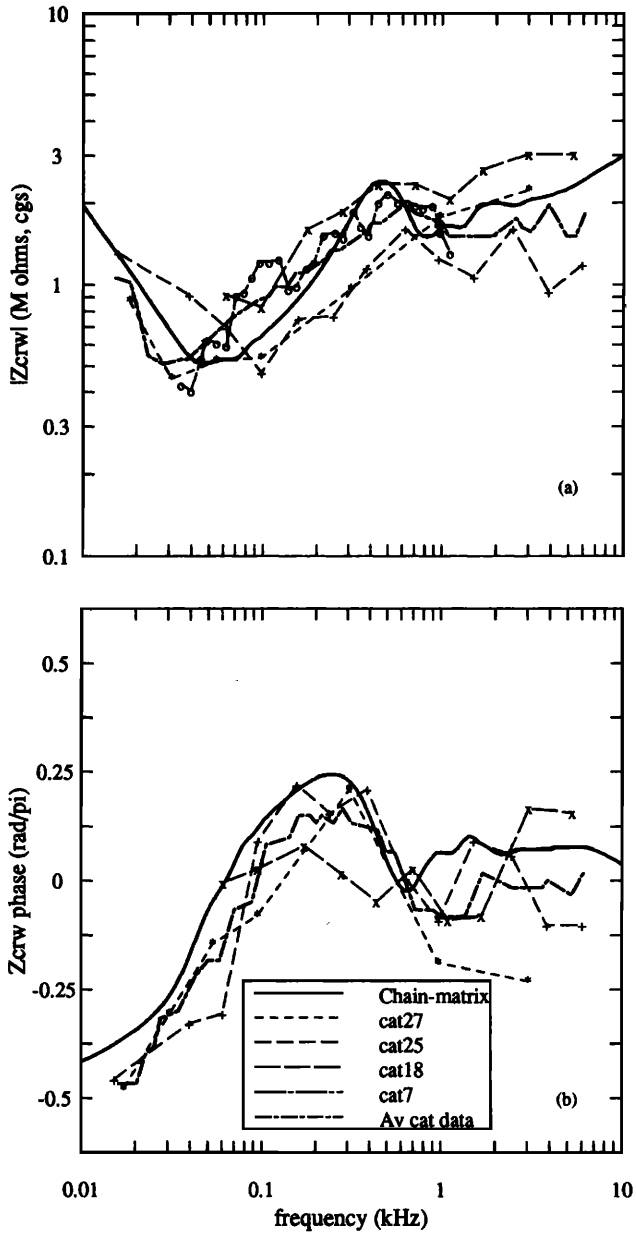

FIG. 15. Comparison with Lynch *et al.*'s measured data. "cat27," "cat25," "cat18," and "cat7" are measurements of $Z_{crw}(\omega)$ on individual cats (Lynch *et al.*, 1982). The "Av cat data" shown here and in previous figures were obtained by Lynch *et al.* by averaging the individual curves. The individual data shows significant interanimal variability. For frequencies greater than 1 kHz, the measured phase is distributed on both sides of zero. This indicates that the individual animal phase is not necessarily resistive, at frequencies above 1 kHz, as one would be lead to believe by looking at the phase of the averaged data. From the present study we conclude that one reason for the inter-animal variability in cochlear input impedance is due to inter-animal differences in the scalae area. Calculation parameters are: $S_m(x)$, $K_0' = 1.7\times10^9$, $K_{rw} = 1.2\times10^8$, and $x_0 = 0.15$ cm.

which the averaged data were obtained. Figure 15 shows the four measurements of Z_c on individual cats by Lynch *et al.* (1982). It is apparent from Fig. 15 that the individual cats show a large amount of interanimal variability. Some of the trends present in the averaged data are more pronounced in each of the individual curves. For frequencies above 1 kHz, the individual phase is positive and negative across animals and would tend to average to zero, leaving a real result. *Thus, for any given animal, Z_c is not necessarily real at frequencies above 1 kHz.*

The model results shown in Fig. 15 are obtained by using parameters of previous sections. The parameters used are: $S_m(x)$ (see Fig. 12), pressure measured at location $x_0 = 0.15$ cm, $\eta = 0.02$, $Z_h = \text{SC}$, $K_0' = 1.7\times10^9$. K_{rw} was increased to 1.2×10^8. A comparison with individual data shows good quantitative agreement. From our modifications to the area function, albeit in a heuristic manner, we have been able to capture some of the detailed structure of the cochlear input impedance. From this exercise we reach the conclusion that individual animal differences in the scala area result in measurable differences in the cochlear input impedance. It was noted that for frequencies above 1 kHz, the interanimal phase is both positive and negative; this variation is most likely due to interanimal differences in the basal region of the scala vestibule area function, variations in transducer placement, or perhaps errors in animal measurements.

IV. EXTENSION TO OTHER SPECIES

To accurately compute the cochlear input impedance, we have proposed a cochlear model that requires the specification of species-dependent parameters such as: the area function of the vestibule, the cochlear map $f_{CF}(x)$, the length of the cochlea x_L, the BM width function $\beta(x)$, the round window stiffness K_{rw}, and the area of the footplate A_{fp}. In addition, one also needs to specify the physical constants for the perilymph such as: viscosity η, and the density ρ. The parameters chosen thus far were for calculating the cochlear input impedance of the cat. Given the model, we now compute the cochlear input impedance for the guinea pig, man, and the chinchilla, and compare our results to those of the cat, for frequencies up to 70 kHz.

The human cochlear map according to Greenwood (1961) is

$$f_{CF}^{man}(x) = 165.4\left[10^{(2.1/x_L)(x_L - x)} - 1\right], \tag{20}$$

the guinea pig cochlear map (Greenwood, 1990) is

$$f_{CF}^{gp}(x) = 350\left[10^{(2.1/x_L)(x_L - x)} - 0.85\right], \tag{21}$$

and the chinchilla cochlear map (Eldredge *et al.*, 1981) is

$$f_{CF}^{ch}(x) = 112.5\left[10^{(2.24/x_L)(x_L - x)}\right]. \tag{22}$$

The area functions for the cat [$S_m(x)$ of Fig. 12], human (Wever, 1949), guinea pig (Dallos, 1970), and the chinchilla (Dallos, 1970) that we have used are shown in Fig. 16. Since round window stiffness measurements for some of these animals are not available, we make comparisons of Z_c rather than Z_{crw}. For this reason, comparisons of our calculated results with measurements of Z_c reported in the literature are meaningful only for frequencies above ≈ 70 Hz. Figure 17 compares Z_c for cat, human, guinea pig, and chinchilla cochleas in the frequency region between 10 Hz and 70 kHz given the areas shown in Fig. 16. The BM stiffness $K_b'(x)$ was modified for other species, as in the case for the cat, so that the calculated cochlear map coincided with the actual cochlear map of either Eq. (20), (21), or (22).

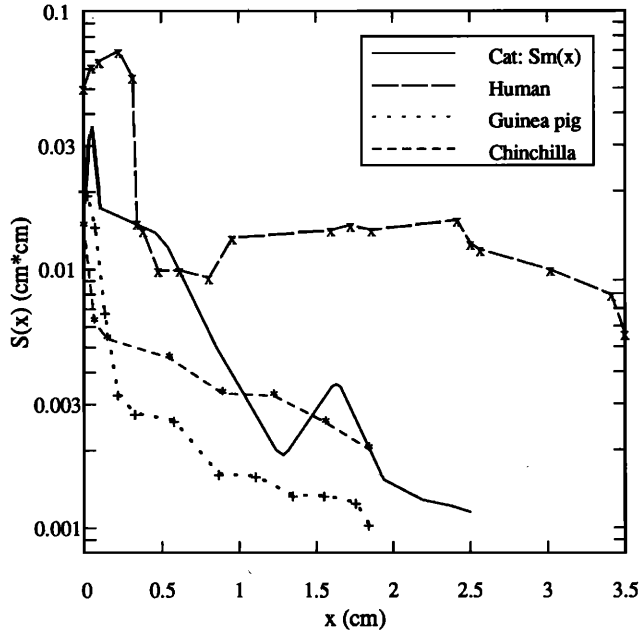

FIG. 16. Inter-species comparison of anatomical measurements of the scala vestibule area. The cat area labeled $S_m(x)$ is from Fig. 12. The human scala vestibule area is from (Wever, 1949). The guinea pig and chinchilla area measurements are from Dallos (1970). The human scala area is the largest and the guinea pig scala area is the smallest.

The species-dependent physical parameters, including the BM stiffness at the base K_0', are shown in Table II.

A. Human impedance

Our model calculations (Fig. 17) show that, below 1 kHz, the human cochlear input impedance slope is approximately 4 dB/oct, reaching a peak at 1.2 kHz of 1.24 MΩ. Between 1.2 and 10 kHz the model $|Z_c|$ starts to decrease with an approximate slope of -6 dB/oct. In comparison, the cochlear input impedance magnitude measured on human temporal bones, is "flat" for 0.6 kHz $< f <$ 2.2 kHz, and the mean value on 11 temporal bones is 0.7 MΩ at 1 kHz (Aritomo and Goode, 1987). Estimates of the measurement error are not reported in (Aritomo and Goode, 1987). Thus, at 1 kHz, our $|Z_c|$ is higher than the measured data by a factor of 1.8 (5.1 dB).

B. Guinea pig impedance

The only reported measurements of guinea pig impedance have been by Dancer and Franke (1980). Since phase measurements were not reported in that study, we compare our theoretical results with their magnitude measurements. Dancer and Franke estimated the impedance from pressure measurements in the first turn of the scala vestibule. In the frequency region between 200 Hz and 2 kHz the measured impedance magnitude is approximately 0.4 MΩ. The slope of the measured impedance is approximately 5 dB/oct for the frequency region between 2 and 5 kHz, and the impedance is approximately 0.8 MΩ near 5 kHz. Above 7 kHz the measured impedance magnitude is approximately 0.4 MΩ.

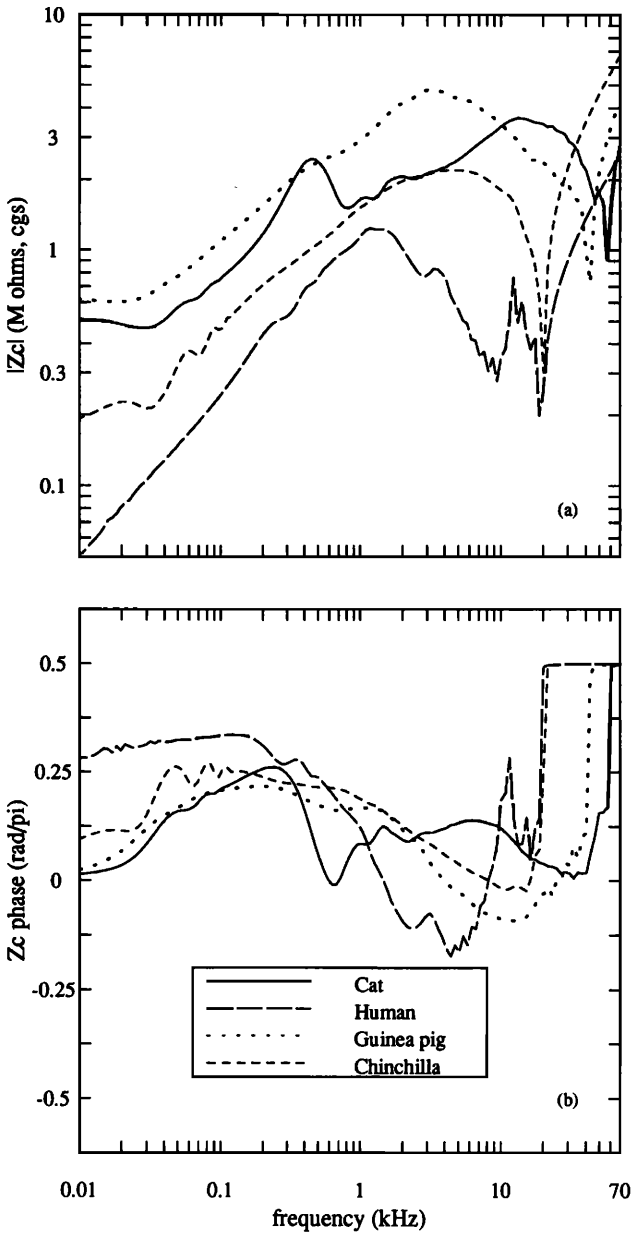

FIG. 17. Interspecies comparison and high-frequency effects of $Z_c(\omega)$. For frequencies just above $f_{max} = f_{CF}(x = 0)$, Z_c becomes completely mass dominated for all four animals. This is a predictable result, since the mass of the fluid and mass of the BM dominates in that frequency region. However, the sudden decrease in $|Z_c|$ for ≈ 10 kHz $< f < f_{max}$ is unexpected. Human Z_c is lowest in magnitude, due to its relatively large scalae area, and the guinea pig Z_c is largest in magnitude due to its relatively small scalae area. Since the human scalae area in the apical region is larger than the other animals, the viscous boundary layer is not as significant for human Z_c as it is for the other animals at low frequencies (below ≈ 150 Hz). Thus the human Z_c is more mass-like than the other animals studied, as may be seen by the phase. The corresponding scalae areas are shown in Fig. 16. The other model parameters are listed in Table II ($\eta = 0.02$, $Z_h = \mathrm{SC}$).

Figure 17 shows that this estimate of the magnitude of the impedance is smaller than our theoretical calculations by as much as a factor of ≈ 6 (15.6 dB). From Fig. 2 of Dancer and Franke (1980), we estimate that their "confidence in-

TABLE II. Species dependent parameters. For chinchilla and man A_{fp} of the cat were used; K_0' is the basilar membrane stiffness at the base. Anatomical parameters for the helicotrema are not required for man, guinea pig, and chinchilla model calculations since a short-circuit helicotrema impedance was used; they are listed here only for comparison to the cat.

Parameter	Cat	Guinea pig	Chinchilla	Man	Units
x_L	2.5[a]	1.85[b]	1.84[c]	3.5[d]	cm
H[g]	0.146	0.161	0.137	0.254	cm
β_0	0.011[f]	0.01[b]	0.023[e]	0.015[h]	cm
β_1	0.56[f]	0.375[b]	0.3[e]	0.329[h]	cm^{-1}
a_h	0.125[i]	0.0084[e]	0.0248[e]		cm
l_h[j]	0.04	0.0284	0.078		cm
A_{fp}	0.0126[k]	0.014[b]			cm^2
K_{rw}	10^8 [k]				dyn/cm^5
K_0'	1.7×10^9	8.3×10^8	4.5×10^8	2.4×10^8	dyn/cm^3

[a] Liberman (1982).
[b] Fernández (1952).
[c] Eldredge *et al.* (1981).
[d] von Békésy (1960, p. 29).
[e] Dallos (1970).
[f] Cabezudo (1978).
[g] $H = 2\sqrt{S_0/\pi}$.
[h] Wever (1949, p. 100).
[i] Mulroy (Lynch *et al.*, 1982, note 11).
[j] $l_h = \pi a_h$.
[k] Lynch *et al.* (1982).

terval" of 95% corresponds approximately to a measurement error of $\pm$ 6 dB. Even with this measurement error our results seem to be outside the range of experimental error.

C. Chinchilla impedance

Recently, Ruggero *et al.* (1990) have reported measurements of Z_c for the chinchilla. They found an impedance of approximately 0.5–0.9 MΩ in the 1-kHz $< f <$ 15-kHz frequency region, and the impedance decreases with an approximate slope of 7 dB/oct below 1 kHz. Our model calculations are greater than the reported values by as much as a factor of 4.4 (12.9 dB). The measured phase decreases from approximately $\pi/4$ at 300 Hz to approximately $\pi/8$ at 3 kHz, in agreement with our calculations. However, for 3 kHz $< f <$ 18 kHz the measured phase starts to increase toward π, whereas the model phase continues toward zero. The model phase is $\pi/2$ for $f >$ 20 kHz. In Ruggero *et al.* (1990) the maximum measurement error was not reported. Note that f_{CF}^{ch} is a straight cochlear map but oscillations in Z_c in the model were substantially reduced due to the presence of viscosity and tapering.

D. Interspecies comparisons

For stimulus frequencies below 10 kHz, it is observed that, of the four species studied, the human impedance is the lowest in magnitude, while the guinea pig impedance is highest in magnitude. For the most part, the human scalae area is greater than the other animals, and the guinea pig scalae area is smaller. These results are consistent with our previous observation (Fig. 9) that the impedance magnitude is inversely proportional to the scalae area.

1. Low-frequency effects

In the previous sections we concluded that the resistive behavior of Z_c below $\approx$150 Hz is due to the interaction of tapering with viscosity. Since the area in the apical region of the human cochlea is significantly larger than other cochleas, the viscous boundary layer thickness is less significant in the human cochlea; thus the human cochlear input impedance is not as resistive at low frequencies as the other animals studied.

2. High-frequency effects

For 10 kHz $< f < f_{max}$, where $f_{max} = f_{CF}(x = 0)$, there is a "dip" or decrease in the impedance for all four species. To our knowledge, this decrease in model impedance has not been previously observed. In all four cases, Z_c abruptly becomes mass dominated for frequencies above f_{max} of the cochlear map. For the cat, man, guinea pig, and chinchilla this occurs at $f_{max} \approx$ 57, 20.7, 43.8, and 19.6 kHz, respectively. Based on heuristic arguments, this mass-dominated region was modeled as M_V in Lynch *et al.* (1982, Fig. 23). In the chain-matrix model, the high-frequency effects of the perilymph fluid mass and organ of Corti mass arise in a natural manner.

If it could be measured, the sharp transition in Z_c near f_{max} of the cochlear map would appear to be a sensitive test of a traveling wave in species such as the turtle or the lizard, where the traveling wave properties are in question.

Most measurements of the cochlear input impedance have tended to be below 20 kHz. A way of verifying these high-frequency results would be to make cochlear input impedance measurements up to and beyond f_{max} of the cochlear map of the specific animal being studied.

V. DISCUSSION

Standing waves exist when there are reflections at both the stapes end and the apical end of the cochlea. The problem of apical reflections has been analyzed in detail. We conclude that the magnitude of apical reflections can be eliminated by using a cochlear map of the form $f_{CF}(x) = A\left[10^{-(\alpha/x_L)(x-x_L)} - 1\right]$. Alternatively, the amplitude of the apical reflections can be substantially reduced by properly accounting for scalae area variations and viscosity in the cochlear model. In such a model, the apical reflections are dissipated by the viscous boundary layer when it is comparable to the tube radius in the apical region of the cochlea. Potential artifacts due to standing waves in nonlinear time-domain models can be controlled by eliminating apical reflections.

By modeling the cochlear input impedance, important insight has been gained regarding mechanisms of the cochlea. Specifically, we have shown that the scalae area function $S(x)$ of the cochlea is important when one is interested in accurately calculating $Z_c(\omega)$. The effect of viscosity is significant for frequencies below those where the viscous boundary layer thickness is comparable to the radius of the scalae in the apical region. For the cat, chinchilla, and guinea pig, this occurred at approximately 150 Hz. The helicotrema boundary condition has been a point of conjecture in cochlear mechanics. We have shown that the helicotrema acous-

tic impedance has an insignificant effect on $Z_c(\omega)$ in comparison to the effects of tapering and viscosity. We conclude that the helicotrema can be approximated as an acoustic short circuit without altering cochlear dynamic results, assuming tapering and viscosity are properly accounted for in the cochlear model. Traditionally, the helicotrema is considered to be the small hole at the apex of the cochlea. However, our model calculations show that, acoustically, the helicotrema extends well into the cochlea.

In answer to the question "What physical mechanisms give rise to R_0 of Fig. 1," we conclude that tapering increases the impedance magnitude and inclusion of perilymph viscosity results in the impedance becoming real as $f \to 0$. For the cat, chinchilla, and guinea pig, the impedance is dominated by the real component for frequencies below approximately 150 Hz. Therefore, the notion that the input impedance depends only upon the properties of the BM close to the stapes, such as in the WKB approximation, is not consistent with the results derived in this paper. Stated in other terms, the reflected wave component is an important and necessary part of the cochlear input impedance calculation.

We have shown that accurate calculations of the cochlear input impedance require accurate specifications of the scala vestibule and scala tympani area functions. A further verification of this result would require more cochlear input impedance measurements along with corresponding anatomical measurements of the area functions.

Sondhi (1981) conjectured that it is possible to gain insight about important BM parameters, such as the BM stiffness function $K_b(x)$, from $Z_c(\omega)$. Testing this idea, with a constant height cochlear model, did not prove to yield physically reasonable results for the stiffness function (Sondhi, 1988). Alternatively, under the assumptions of full knowledge of the BM stiffness $K_b(x)$ derived from the cochlear map, it might be possible to recover the area function $S(x)$ from the input impedance measurements by Sondhi's acoustic inverse method.

VI. SUMMARY

A nonuniform transmission line model of the cochlea is formulated as a cascade of two-port chain matrices. This model includes the effects due to the spatial variations in scalae area, the viscous perilymph, spatial variations in the basilar membrane partition, and the impedance of the helicotrema.

Figure 18 graphically depicts some of the main points of this paper. The curve with ($S = 0.0167$ cm^2) is the only curve with constant scalae area. The other curves are with an area that is a close approximation to anatomical measurements of the scalae area $S_m(x)$. It is clear from Fig. 18 that, for frequencies below about 1 to 2 kHz, the magnitude of the cochlear input impedance with a constant scalae area diverges from the model calculations with realistic scalae area. For frequencies above $\approx$150 Hz, there is good quantitative agreement between the data and our model calculation with a realistic scalae area (see Fig. 15). The amplitude oscillations in Z_c below $f_{CF}^{cl}(x_L)$ are present in both the constant scalae area model and the model with the realistic scalae area. These oscillations indicate the presence of apical reflec-

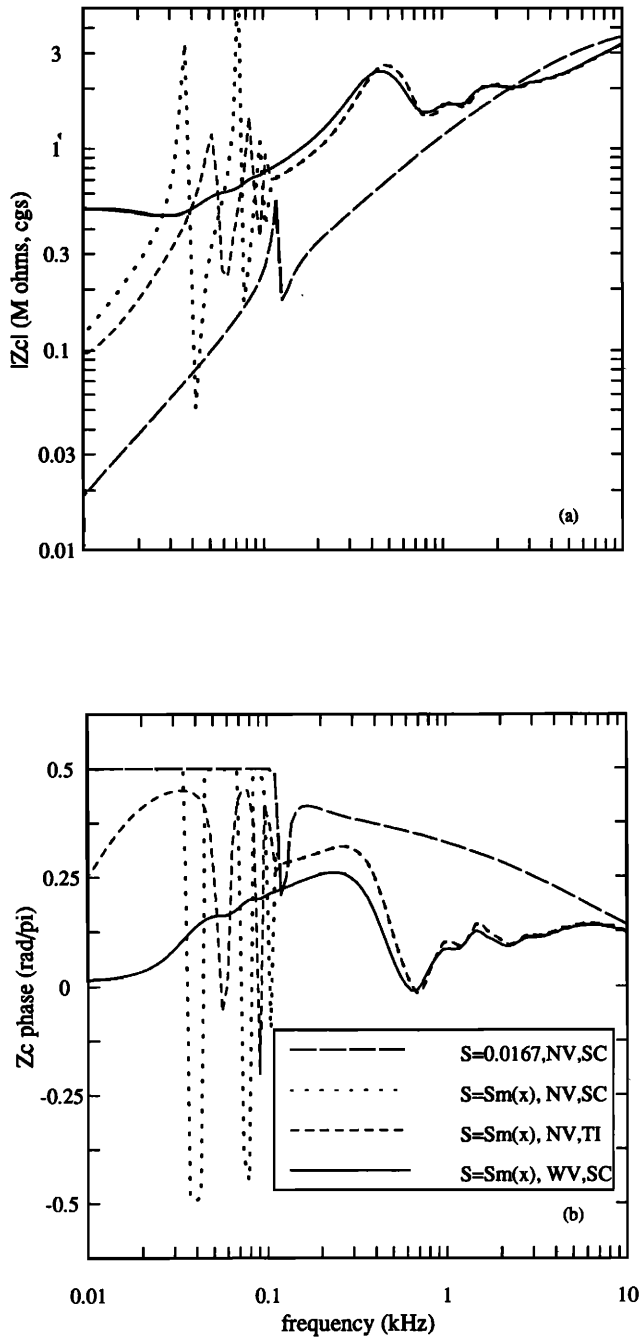

FIG. 18. Summary of results: $Z_c(\omega)$ with constant scalae area, no viscosity, and a helicotrema short circuit is labeled as ($S = 0.0167$, NV,SC). The sudden jump in Z_c near 100 Hz is due to apical reflections resulting from the low-frequency limit of the cochlear map $f_{CF}^{cl}(x_L)$. The other calculations of Z_c use the more realistic scalae area $S_m(x)$ of Fig. 12. For frequencies below about 1 to 2 kHz the constant scalae area model magnitude of Z_c diverges from the model calculations with realistic scalae area. For all cases having scalae area $S_m(x)$, model results are in good agreement with measured data for frequencies above $\approx$150 Hz (see Fig. 15). Below $f_{CF}^{cl}(x_L)$, the large oscillations in Z_c are due to apical reflections. Adding a tube impedance, for the helicotrema, has the effect of changing the nature of the reflections, but it fails to remove them. After including perilymph viscosity (WV), two important result emerge for frequencies below $\approx$150 Hz. First, the phase indicates that Z_c is resistance dominated. Second, the apical reflections have dissipated. Viscous effects are important when the scalae radius becomes comparable to the viscous boundary layer.

tions. In the realistic scalae area case, the magnitude of the reflections are much greater due to an increase in impedance mismatch between the scalae and the helicotrema. Although adding a tube impedance, for the helicotrema, affects the nature of the apical reflections, it fails to remove them. When perilymph viscosity is included in the model, two important effects are observed for frequencies below ≈ 150 Hz: First, the impedance starts to become more and more resistive as frequency decreases and, second, the apical reflections have dissipated. These effects are due to the viscous boundary layer becoming comparable to the scalae radius in apical region of the cochlea.

ACKNOWLEDGMENTS

We thank Dr. John J. Rosowski of Eaton–Peabody Laboratory for several critical readings of this paper, leading to numerous improvements. The authors would like to thank AT&T Bell Laboratories for providing financial support to enable author SP to do his Ph.D thesis at Bell Laboratories Acoustics Research Department. The authors are also grateful to Professor Nenad M. Marinovic of City College for giving SP encouragement and freedom to do research in cochlear mechanics.

APPENDIX A: LOSSY CYLINDRICAL TUBE THEORY

Lossy transmission-line theory describes the acoustical properties of a tube, having section length Δ and area S, in terms of the per unit length series acoustic impedance $Z(\omega)$ and the per unit length shunt acoustic admittance $Y(\omega)$. This theory, originally formulated by Kirchhoff (1868), is a linear acoustic theory which includes viscous and thermal boundary layers to account for the propagation of losses. To calculate Z and Y, one needs to know the scalae radius $r_0(x) = \sqrt{S(x)/\pi}$, and the viscous and thermal boundary layer thickness (see below), which are proportional to $\omega^{-1/2}$. Given Z and Y, one may calculate the propagation "constant" (which is not a constant), and the characteristic impedance using standard transmission-line formulas.

1. Lossy series impedance

The per unit length series acoustic impedance Z is given by (Benade, 1968, Flanagan, 1983; Keefe, 1984)

$$Z(x,\omega) = R_v(x,\omega) + sL(x,\omega) = s\rho/S(x)(1 - F_v), \quad \text{(A1)}$$

where the functions R_v and L are defined as the resistive and inductive parts of Z. The viscous factor F_v is given by

$$F_v = 2J_1(r_v\sqrt{-j})/r_v\sqrt{-j}J_0(r_v\sqrt{-j}). \quad \text{(A2)}$$

In the preceding equation,

$$r_v = r_0/\delta \quad \text{(A3)}$$

is the ratio of the tube radius $r_0 = \sqrt{S/\pi}$ and the viscous boundary layer thickness

$$\delta = \sqrt{\eta/\rho\omega}. \quad \text{(A4)}$$

2. Lossy shunt admittance

The per unit length shunt acoustic admittance Y is defined as (Benade, 1968; Flanagan, 1983; Keefe, 1984)

$$Y(x,\omega) = G(x,\omega) + sC(x,\omega) = [sS(x)/\rho c^2][1 + (\gamma - 1)F_t], \quad \text{(A5)}$$

where the thermal factor F_t is given by

$$F_t = 2J_1(r_t\sqrt{-j})/r_t\sqrt{-j}J_0(r_t\sqrt{-j}). \quad \text{(A6)}$$

where

$$r_t(x) = r_v\sqrt{N_p}.$$

The tube radius, normalized by the thermal boundary layer thickness, is r_t and is related to r_v by the Prandtl number $N_p = \eta c_p/\kappa$. The functions G and C are defined as the conductive and compliant parts of Y.

The thermodynamical constants used in the foregoing equations are listed in Table AI. The Bessel functions J_0 and J_1 must be calculated at a $-\pi/4$ angle in the complex plane since r_v and r_t are real and $\arg(\sqrt{-j}) = -\pi/4$. Benade (1968), Keefe (1984), and others have given results leading to small and large tube radius approximations for F_v and F_t. In the interest of preserving the accuracy of Eqs. (A1) and (A5), since any error might propagate in the recursive solutions, we calculate the Bessel functions of complex arguments with double precision accuracy.

The real and imaginary parts of $Y(x,\omega)$ are defined as $G(x,\omega)$ and $\omega C(x,\omega)$. The real and imaginary part of $Z(x,\omega)$ are defined as $R_v(x,\omega)$ and $\omega L(x,\omega)$. We further break down the definition of L into two components, L_0 nd L_v. The fluid inertia term L_0 increases from the base to the apex. Since F_v is complex, it is evident from Eqs. (A1) and (A2) that the presence of viscosity gives rise to a real part and a reactive part. By definition, $R_v(x,\omega)$ is the increased resistance, and $L_v(x,\omega)$ is the added mass due to viscosity. For the inviscid case ($\eta \to 0$), $r_v \to \infty$, and from the large argument approximation to the Bessel functions (Morse and Feschbach, 1953, p. 1321), $F_v \to 0$. As a result, $R_v \to 0$ and $L \to L_0 = \rho/S(x)$. In using the above results, we assume that S is constant over a section length Δ.

TABLE AI. Thermodynamic constants for perilymph.

Name	Parameter	Value	Units
Density	ρ	1	g/cm^3
Viscosity	η	0.02	g cm^{-1} s^{-1}
Sound speed	c	1.5×10^5	cm/s
Prandtl number	N_p	7.02	dimensionless
Ratio of specific heats	γ	1	dimensionless

APPENDIX B: DERIVATION OF BASILAR MEMBRANE IMPEDANCE

The equations describing the parameters corresponding to a BM with fourth-order partition dynamics are summarized here (Allen, 1980). The BM specific impedance is

$$Z_{BM}(x,s) = s(m_T + m_{oc}) + K_b(x)/s + G^2(x) \times H_T(x,s), \quad \text{(B1)}$$

where K_b is the BM stiffness, m_{oc} is the organ of Corti (OC) mass, m_T is the mass of the tectorial membrane, and $G(x)$ is the shear gain. The transduction filter $H_T(x,s)$ is defined as

$$H_T(x,s) = \frac{(r_c + k_c/s)(k_T/s + r_T + sm_T)}{(k_c + k_T)/s + (r_c + r_T) + sm_T}, \quad \text{(B2)}$$

where k_c and r_c are the stereocilia stiffness and damping, and similarly k_T and r_T are the tectorial membrane stiffness and damping. Equation (B2) can be rendered dimensionless by redefining $k_c(x)$, $k_T(x)$, $r_c(x)$, $r_T(x)$ in terms of $\omega_z(x)$, $\omega_p(x)$, $\zeta_z(x)$, $\zeta_p(x)$ (Allen, 1980), where ω_p, ω_z are the pole, zero frequencies of the transduction filter and ζ_p, ζ_z are the damping factors associated with the pole and the zero. Equation (B2) then becomes

$$H_T(x,s) = \frac{G(x)}{\Lambda^2}\left(\frac{(s/\omega_z)^2 + 2\zeta_z(s/\omega_z) + 1}{(s/\omega_p)^2 + \zeta_p(s/\omega_p) + 1}\right), \quad \text{(B3)}$$

where

$$\Lambda = \omega_p/\omega_z. \quad \text{(B4)}$$

In this form, one needs only to specify $\omega_z(x)$, $\omega_p(x)$, $\zeta_z(x)$, $\zeta_p(x)$ and the gain $G(x)$ to calculate Eq. (B2). To estimate the parameters we have assumed the following:

$$\omega_p(x) = 1.3\omega_{CF}(x) \quad \text{(B5)}$$

$$\omega_z(x) = 0.65\omega_{CF}(x) \quad \text{(B6)}$$

$$\zeta_p(x) = 0.3 \quad \text{(B7)}$$

$$\zeta_z(x) = 0.5 \quad \text{(B8)}$$

$$G(x) = 0.5\exp\{(x - x_L)/x_L\} \quad \text{(B9)}$$

and

$$\omega_{CF}(x) = 2\pi f_{CF}(x), \quad \text{(B10)}$$

where $f_{CF}(x)$ is the cochlear map. It is assumed in Eqs. (B5) and (B6) that the pole and the zero lie above and below $f_{CF}(x)$. K_b in Eq. (B1) is evaluated according to

$$K_b(x) = (m_T + m_{oc})\omega_{CF}^2 - m_T\omega_p^2 \times [1 + (\omega_z/\omega_p)^2]G(x) \times \{[(\omega_z/\omega_{CF})^2 - 1]/[(\omega_p/\omega_{CF})^2 - 1]\}. \quad \text{(B11)}$$

The specific mass of the organ of Corti is

$$m_{oc} = \rho_{oc}h_{oc}(x), \quad \text{(B12)}$$

and the specific mass of the tectorial membrane (TM) is

$$m_T = \rho_T h_T(x), \quad \text{(B13)}$$

where ρ_{oc} and ρ_T are densities of the OC and the TM, $h_{oc}(x)$ is the height of the OC, and $h_T(x)$ is height (thickness) of the TM. We assume that $\rho_{oc} = \rho_T = \rho$ the density of water. With these assumptions, $m_{oc} + m_T$ is 0.04 g/cm^2. The cochlear map from the model was generated by plotting the peak location of the BM velocity as a function of the input frequency. Using Eq. (B11), the resulting calculated cochlear map fell below (in frequency) the actual cochlear map [either Eq. (15), (16), or (17)] by $\approx 1/\sqrt{3}$. This deficiency in the model of the basilar membrane stiffness $K_b(x)$ [Eq. (B11)] was accounted for by multiplying $K_b(x)$ by a constant (≈ 3) so as to make the model cochlear map and desired cochlear map coincide.

The total stiffness in Z_{BM} [Eq. (B1)] is

$$K(x) = K_b(x) + G^2(x)\{k_c(x)k_T(x)/ \times [k_c(x) + k_T(x)]\}. \quad \text{(B14)}$$

For the parameters chosen, $G^2(x) < 1$, and the parallel combination of k_c and k_T is typically less than 0.1 of $K_b(x)$. Thus the second term of Eq. (B14) has a negligible effect [i.e., $K(x) \approx K_b(x)$].

[1]Here, $Z_{BM}(x)$ was formulated for the rectangular coordinate system with height H cm. The present model is formulated in the cylindrical coordinate system. The impedance transformation was necessary for the results of the two formulations to be equivalent (Viergever, 1980, p. 69).

[2]The model of Allen (1977) was formulated for a two-dimensional cochlear model (fourth-order system of equations in the notation of that paper). The formulation was sufficiently general enough so as to allow a one-dimensional formulation (second-order system of equations), as is appropriate for the present case.

Allen, J. B. (1977). "Cochlear micromechanics—a mechanism for transforming mechanical to neutral tuning within the cochlea," J. Acoust. Soc. Am. **62**, 930–939.

Allen, J. B. (1979). "Cochlear models—1978," in *Models of the Auditory System and Related Signal Processing Techniques*, edited by M. Hoke and E. de Boer, Scand. Audiol. Suppl. **9**, 1–16.

Allen, J. B. (1980), "Cochlear micromechanics—A physical model of transduction," J. Acoust. Soc. Am. **68**, 1660–1670.

Aritomo, H., and Goode, R. L. (1987). "Cochlear input impedance in fresh human temporal bones," Am. Acad. Otolaryngol. abs.

Benade, A. H. (1968). "On the propagation of sound waves in a cylindrical conduit," J. Acoust. Soc. Am. **44**, 616–623.

Beranek, L. L. (1954). *Acoustics* (McGraw-Hill, New York).

Cabezudo, L. M. (1978). "The ultrastructure of the basilar membrane in the cat," Acta Otolaryngol. **86**, 160–175.

Dallos, P. (1970). "Low-frequency auditory characteristics: Species dependence," J. Acoust. Soc. Am. **48**, 489–499.

Dallos, P. (1973). *The Auditory Periphery—Biophysics and Physiology* (Academic, New York).

Dancer, A., and Franke, R. (1980). "Intracochlear sound pressure measurements in guinea pigs," Hear. Res. **2**, 191–205.

Diependaal, R. (1988). "Nonlinear and active cochlear models: analysis and solution methods," Ph.D. thesis, Delft University.

Eldredge, D. H., Miller, J. D., and Bohne, B. A. (1981). "A frequency-position map for the chinchilla cochlea," J. Acoust Soc. Am. **69**, 1091–1095.

Fahey, P. F., and Allen, J. B. (1985). "Nonlinear phenomena as observed in the ear canal and at the auditory nerve," J. Acoust. Soc. Am. **77**, 599–612.

Fernández, C. (1952). "Dimensions of the cochlea (guinea pig)," J. Acoust. Soc. Am. **24**, 519–523.

Flanagan, J. L. (1983). *Speech Analysis Synthesis and Perception* (Springer-Verlag, Berlin), 2nd ed.

Greenwood, D. D. (1961). "Critical bandwidth and the frequency coordinates of the basilar membrane," J. Acoust. Soc. Am. **33**, 1344–1356.

Greenwood, D. D. (1990). "A cochlear frequency-position function for several species—29 years later," J. Acoust. Soc. Am. **87**, 2592–2605.

Guinan, J. J., and Peake, W. T. (1967). "Middle-ear characteristics of anesthetized cats," J. Acoust. Soc. Am. **41**, 1237–1261.

Hall, J. L. (1974). "Two-tone distortion products in a nonlinear model of the basilar membrane," J. Acoust. Soc. Am. **56**, 1818–1828.

Hubbard, A. E., and Geisler, C. D. (1972). "A hybrid-computer model of the cochlear partition," J. Acoust. Soc. Am. **51**, 1895–1903.
Keefe, D. H. (1984). "Acoustical wave-propagation in cylindrical ducts: Transmission line parameter approximation for isothermal and nonisothermal boundary conditions," J. Acoust. Soc. Am. **75**, 58–62.
Kemp, D. T. (1978). "Stimulated acoustic emissions from within the human auditory system," J. Acoust. Soc. Am. **64**, 1386–1391.
Kemp, D. T. (1979). "Evidence of mechanical non-linearity and frequency selective wave amplification in the cochlea," Arch. Otorhinolaryngol. **224**, 37–45.,
Kemp, D. T. (1980). "Towards a model of the origin of cochlear echoes," Hearing. Res. **2**, 533–548.
Kim, D. O., Molnar, C. E., and Matthews, J. W. (1980). "Cochlear mechanics: Nonlinear behavior in two-tone responses as reflected in cochlear-nerve responses and in ear-canal sound pressure," J. Acoust. Soc. Am. **67**, 1704–1721.
Kirchhoff, G. (1868). "On the influence of heat conduction in a gas on sound propagation," Ann. Phys. Chem. **134**, 177–193.
Koshigoe, S., Kwok, W. K., and Tubis, A. (1983). "Effects of perilymph viscosity on low-frequency intracochlear pressures and the cochlear input impedance of the cat," J. Acoust. Soc. Am. **74**, 486–492.
Lesser, M. B., and Berkley, D. A. (1972). "Fluid mechanics of the cochlea, Part 1," J. Fluid Mech. **51**, 497–512.
Liberman, M.C. (1982). "The cochlear frequency map for the cat: Labeling auditory-nerve fibers of known characteristic frequency," J. Acoust. Soc. Am. **72**, 1441–1449.
Lynch, T. J., III, Nedzelnitsky, V., and Peake, W. T. (1982). "Input impedance of the cochlea in cat," J. Acoust. Soc. Am. **72**, 108–130.
Matthews, J. W. (1980). "Mechanical modeling of nonlinear phenomena observed in the peripheral auditory system," Ph.D. thesis, Washington University, St. Louis, MO.
Moller, A. R. (1965). "An experimental study of the acoustic impedance of the middle ear and its transmission properties," Acta Otolaryngol. **60**, 129–149.
Morse, P. M., and Feschbach, H. (1953). *Methods of Theoretical Physics, Part II* (McGraw-Hill, New York), p. 1321.
Nedzelnitsky, V. (1980). "Sound pressures in the basal turn of the cat cochlea," J. Acoust. Soc. Am. **68**, 1676–1689.
Neely, S. T., and Kim, D. O. (1986). "A model for active elements in cochlear biomechanics," J. Acoust. Soc. Am. **79**, 1472–1480.
Peterson, L. C., and Bogert, B. P. (1950). "A dynamical theory of the cochlea," J. Acoust. Soc. Am. **22**, 369–381.
Pierce, A. D. (1989). *Acoustics—An Introduction to Its Physical Principles and Applications* (Acoustical Society of America, New York), Chap. 7.
Puria, S., and Allen, J. B. (1988). "Effects of scalae tapering, perilymph viscosity, helicotrema and the cochlear map function on models of the cochlea," J. Acoust Soc. Am. Suppl. 1 **84**, S54.
Puria, S., and Allen, J. B. (1989). "Effects of scalae tapering, perilymph viscosity, helicotrema and the cochlear map function on models of the cochlea," Assoc. for Res. Oto-Laryngol. Abs. **12**, 142.
Rosowski, J. J., Peake, W.T., and Lynch, T. J., III (1984). "Acoustic input-admittance of the alligator-lizard ear: Nonlinear features," Hear. Res. **16**, 205–223.
Ruggero, M. A., Rich, N. C., Robles, L., and Shivapuja, B. G. (1990). "Middle ear response in the chinchilla and its relationship to mechanics at the base of the cochlea," J. Acoust. Soc. Am. **87**, 1612–1629.
Shera, C. A., and Zweig, G. (1991). "Asymmetry suppresses the cochlear catastrophe," J. Acoust. Soc. Am. **89** (to be published).
Sondhi, M. M. (1978). "Method for computing motion in a two-dimensional cochlear model," J. Acoust. Soc. Am. **63**, 1468–1477.
Sondhi, M. M. (1981). "Acoustical inverse problem for the cochlea," J. Acoust. Soc. Am. **69**, 500–504.
Sondhi, M. M. (1988). Personal communication.
Tonndorf, J., Khanna, S. M., and Fingerhood, B. J. (1966). "The input impedance of the inner ear in cats," J. Acoust. Soc. Am. **75**, 752–763.
Viergever, M. A. (1978). "Basilar membrane motion in a spiral-shaped cochlea," J. Acoust. Soc. Am. **64**, 1048–1053.
Viergever, M. A. (1980). "Mechanics of the inner ear," Ph.D. thesis, Delft U. P., Delft, The Netherlands, p. 69.
Viergever, M.A. (1988). "Asymmetry in reflection of cochlear waves," in *Auditory Frequency Selectivity*, edited by Brian C. J. Moore and Roy D. Patterson (A NATO Advanced Research Workshop).